NASA CONTRACTOR REPORT

NASA CR-424

RESEARCH STUDY OF THE VORTEX VALVE FOR MEDIUM-TEMPERATURE SOLID PROPELLANTS

by W. D. Holt and J. G. Rivard

Prepared under Contract No. NAS 1-4158 *by*
THE BENDIX CORPORATION
Southfield, Mich.
for Langley Research Center

NATIONAL AERONAUTICS AND SPACE ADMINISTRATION • WASHINGTON, D. C. • APRIL 1966

RESEARCH STUDY OF THE VORTEX VALVE FOR MEDIUM-TEMPERATURE SOLID PROPELLANTS

By W. D. Holt and J. G. Rivard

Prepared under Contract No. NAS 1-4158
THE BENDIX CORPORATION
Southfield, Mich.

for Langley Research Center

NATIONAL AERONAUTICS AND SPACE ADMINISTRATION

For sale by the Clearinghouse for Federal Scientific and Technical Information
Springfield, Virginia 22151 – Price $1.20

TABLE OF CONTENTS

LIST OF ILLUSTRATIONS

LIST OF TABLES

FOREWORD

The Bendix Corporation, Research Laboratories Division, has completed a research study of the applicability of the vortex valve principle to a solid propellant, hot-gas secondary injection control system. This work was performed for the National Aeronautics and Space Administration under Contract NAS 1-4158.

The study was initiated on July 10, 1964, and completed June 30, 1965. Work was conducted under the program management of Mr. John Riebe of the Langley Research Center, Langley Station, Hampton, Virginia, and performed by the Attitude Controls Group of the Energy Conversion and Dynamic Controls Laboratory.

GLOSSARY

A = Area (in.^{2})

- A_a = annular
- A_{br} = regulator valve bias control
- A_{br}' = regulator bias orifice
- A_c = vortex valve control injector
- A_o = load
- A_{op} = power valve flow measuring orifice
- A_{or} = regulator valve flow measuring orifice
- A_s = vortex chamber outlet orifice
- A_{sp} = power valve outlet orifice
- A_{sr} = regulator valve outlet orifice
- A_s' = supply pressure dropping orifice
- A_9 = pilot valve control

C = Thermodynamic gas constant ($\sqrt{°R}$/sec)

- C_d = flow coefficient of discharge (dimensionless)

C^* = Sonic velocity (in./sec)

c = Pneumatic capacitance (in.^{2})

D = Diameter (in.)

- D_{br}' = regulator bias orifice
- D_c = vortex valve control injector
- D_{ch} = vortex chamber, outer
- D_o = load orifice
- D_s = vortex chamber outlet orifice
- D_s' = supply pressure dropping orifice

f_1 = Orifice flow function (dimensionless)

g = Gravitational acceleration (in./sec^2)

K = Control injector offset (in.)

k = Ratio of specific heats (dimensionless)

L = Vortex chamber length (in.)

M = Mach number

$\overline{m}$ = Molecular weight (lb/mole)

P = Pressure ($lb/in.^2$)

- P_a = ambient
- P_{br} = regulator bias
- P_c = control
- P_{cl} = load
- P_d = downstream
- P_o = vortex valve outlet
- P_{op} = power valve outlet
- P_{or} = regulator valve outlet
- P_s = supply
- P_s' = gas generator
- P_u = upstream

R = Gas constant (in./°R)

$\overline{R}$ = Universal gas constant (in.-lb/mole°R)

s = Laplace operator (sec^{-1})

T = Temperature (°F)

- T_u = upstream

V = Volume ($in.^3$)

$\overset{\vee}{V}$ = Velocity (in./sec)

$\dot{W}$ = Weight flow rate (lb/sec)

- $\dot{W}_{bl}$ = relief valve
- $\dot{W}_{br}$ = regulator bias
- $\dot{W}_{br}'$ = $\dot{W}_{br} + \dot{W}_{bl}$
- $\dot{W}_c$ = power valve control
- $\dot{W}_{N_2}$ = Nitrogen

$\dot{W}_{OMAX}$ = hot gas

$\dot{W}_{o}$ = total

$\dot{W}_{op}$ = power valve load

$\dot{W}_{or}$ = regulator valve load

$\dot{W}_{s}$ = supply to vortex valves

$\dot{W}_{sp}$ = power valve supply

$\dot{W}_{sr}$ = regulator valve supply

$\dot{W}_{s}'$ = gas generator

Δ_i = Torque motor differential current (amperes)

τ = Time constant (sec)

ω = Frequency (rad/sec)

SUMMARY

This project successfully demonstrated a fluid state control system incorporating vortex valves for throttling the flow from a solid propellant gas generator. The single axis injection system tested would be capable of providing secondary injection thrust vector control using 2000°F gas.

Six hot-gas firings were made. The gas generator supplied a flow of 1.0 lb/sec for 30 seconds. This system incorporated two vortex valves in parallel, functioning together as a flow divider circuit. One of the vortex valves utilizes active control, the other acting essentially as a pressure regulator maintaining the supply pressure constant by effectively bypassing flow when the power valve is throttled. This system demonstrated a flow modulation capability in excess of 4 to 1. The particular system concept selected, using active control on only one vortex valve, does not produce the desired total system performance. A better system approach would be to use active control on both vortex valves and operate essentially in a push-pull mode. The system dynamic response was evaluated with sinusoidal and transient inputs. At 30 cps the amplitude attenuation was -4 db and the phase lag was 28 degrees. The frequency response of the basic vortex valve is fast enough so that the system dynamics are dominated by the associated manifold volume compressibility time constants.

The control system components and associated hardware functioned as desired. The performance of the vortex valve did not change during a 30-second hot-gas test, indicating insensitivity to thermal expansion. A composite structure of high-density graphite backed with asbestos-phenolic eliminated erosion in the supply manifold.

Cold-gas testing of a one-sixth scale model vortex valve was conducted to optimize the configuration and performance of the vortex power valve and vortex regulator valve for the selected system. The normalized performance, with regard to gains and flow modulation range, was practically identical for hot- and cold- gas tests. The two vortex valves required complimentary characteristics, achieved by variation in the vortex valve geometry. This parameter variation experience resulted in further insight into the basic knowledge of vortex valve technology and control system performance.

The logical extension of this program is to develop a fluid state control system using high-temperature (6000°F) aluminized solid propellant gases. Eventually, a direct engine bleed, fluid state, secondary injection thrust vector control system should provide a light-weight system with inherent simplicity and high reliability.

INTRODUCTION

The program described in this report was concerned with establishing the feasibility of throttling the flow of high-temperature, contaminated gases with a vortex valve. The work has been accomplished using a 2000°F solid propellant gas generator, with a flow rate of 1 lb/sec. The ultimate goal for this program is to develop a fluid-state secondary injection thrust vector control system with better reliability and performance than that realized from mechanical valve, flow control systems.

Vortex Valve Technology

A basic fluid state research and development effort has been conducted at the Bendix Research Laboratories on vortex valve components and systems. The following material provides background on basic vortex valve technology. Additional material providing an analytical description of the vortex valve is available in Reference (1).

The vortex amplifier is a fluid state control element requiring no moving mechanical parts. A schematic model of a rudimentary vortex amplifier along with typical performance characteristics is shown in Figure A. The supply flow (P_s) is introduced radially into the cylindrical chamber. The maximum valve flow is determined by an outlet orifice at the center of the chamber. In the absence of control flow, all of the supply flow is radial. When a control flow is introduced into the cylindrical chamber at a point tangent to the outer wall, the momentum rate of the control flow (weight flow times velocity) imparts a rotational flow component to the supply flow as it passes the region of

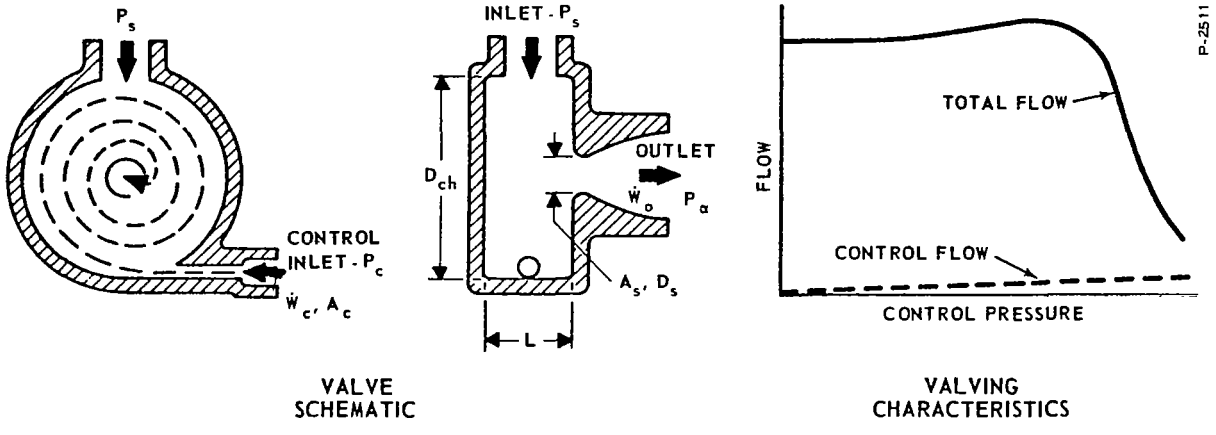

Figure A - Schematic Model of a Vortex Valve

control flow injection. The supply flow thus acquires a tangential velocity component in addition to radial velocity. As the flow proceeds toward the center of the amplifier, the tangential velocity increases to conserve angular momentum. In the vortex amplifier this tangential velocity increase is attenuated by the viscous coupling of the fluid; however, sufficient velocity build up can be achieved which results in a centrifugal pressure drop, providing a mechanism for flow amplification. A small change in control flow results in a relatively large change in total valve flow; typical gains are 100. Near the outlet orifice the flow field changes from a simple two-dimensional vortex flow into a three-dimensional flow as the fluid leaves the orifice. The maximum tangential and radial velocities occur near the center of the vortex chamber.

A purely analytical approach to the general solution of a physical three-dimensional fluid flow is not practical. The internal losses in the valve due to viscous drag are not predictable by purely analytical means. Simplified analysis based on a number of assumptions has verified simple basic experiments. This analysis can serve as a guide in the initial design of vortex devices and provide an insight into the basic performance capabilities and limitations of the vortex amplifier.

The elementary configuration shown in Figure A has been modified as shown in Figure B. The supply flow, instead of being admitted to the vortex chamber at one location, is introduced through an annular slot at the periphery of the vortex chamber. This configuration provides a uniform sheet of supply

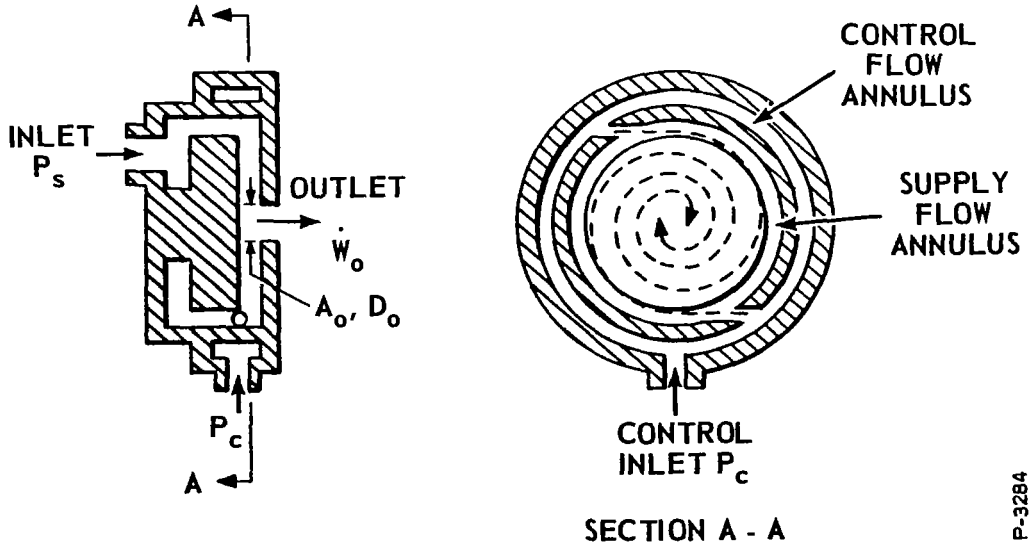

Figure B - Vortex Valve - Button Configuration

flow over the button which induces more uniform mixing of the control and supply flows for better valve performance. The valve performance is also improved by introducing the control flow at various locations about the periphery.

A method of plotting vortex valve control characterisitcs which permits graphical representation of load-flow characteristics is shown in Figure C. The curve defining maximum flow is the orifice flow of the vortex valve with no control flow. The loci within the maximum flow curve represent operation at constant control flow with a variation in supply pressure. This generalized plot can be used in conjunction with appropriate load lines to predict system characteristics.

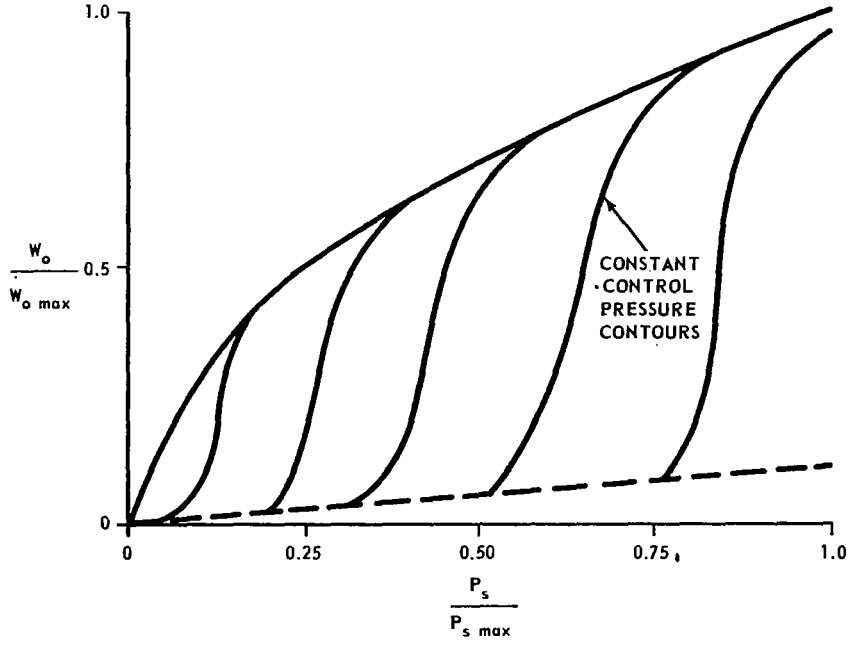

Figure C - Vortex Valve Flow Characteristics

SYSTEM CONCEPT AND ANALYSIS

System Circuit Selection

A schematic of the system selected for demonstration of single-axis thrust vector control is shown in Figure 1. This particular design was selected from three potential configurations because it was estimated to be the simplest and, therefore, the most reliable system configuration. Thus, it would be the most direct approach for demonstrating the secondary injection thrust vector control system concept using fluid state elements.

The system includes two vortex valves in parallel, which direct the flow from a 2000°F Solid Propellant Gas Generator. The vortex valves are separated from the SPGG by pressure dropping orifices. These orifices provide the required pressure differential between the vortex valve control, or bias pressure, and the vortex valve supply. The vortex regulator valve bias is controlled by varying the individual bias trim orifices which set the initial swirl conditions in both the power and regulator vortex valve chambers. The control flow to the power valve is modulated by the torque motor controlled flapper-nozzle pilot stage. An electrical signal to the pilot valve torque motor causes a displacement of the flapper relative to the pilot valve nozzle. This vents the chamber between the pilot stage upstream orifice and the vortex valve control port. Venting the control plenum chamber reduces the control flow to the power valve, which reduces the vortex swirl and increases the power valve flow.

The supply flow from the gas generator is divided between the vortex power valve and the vortex regulator valve. The increase in flow through the power valve reduces the supply pressure to the regulator valve, causing the regulator valve vorticity, or swirl, to increase. This is inherent in the operation because the control bias pressure is maintained constant and, with a decrease in supply pressure, the valve impedance increases. A new equilibrium supply pressure level is reached for any given power valve flow condition.

The system used for both hot- and cold-gas test evaluation is shown in Figure 2. The control of the power valve was accomplished using a mechanical poppet valve for static tests and the flapper-nozzle valve for dynamic tests. The same basic system, redesigned for flight weight, is shown in the Figure 3 layout drawing.

Two other configurations (Figures 4 and 5) were considered before selecting the combination utilizing a power valve and regulator valve. The staged configuration (Figure 4) was eliminated as being too complex for the first-phase feasibility demonstration. This system incorporates vortex chamber bleed control to allow control at pressures lower than supply pressure. It has been demonstrated, but very little development has been accomplished. The

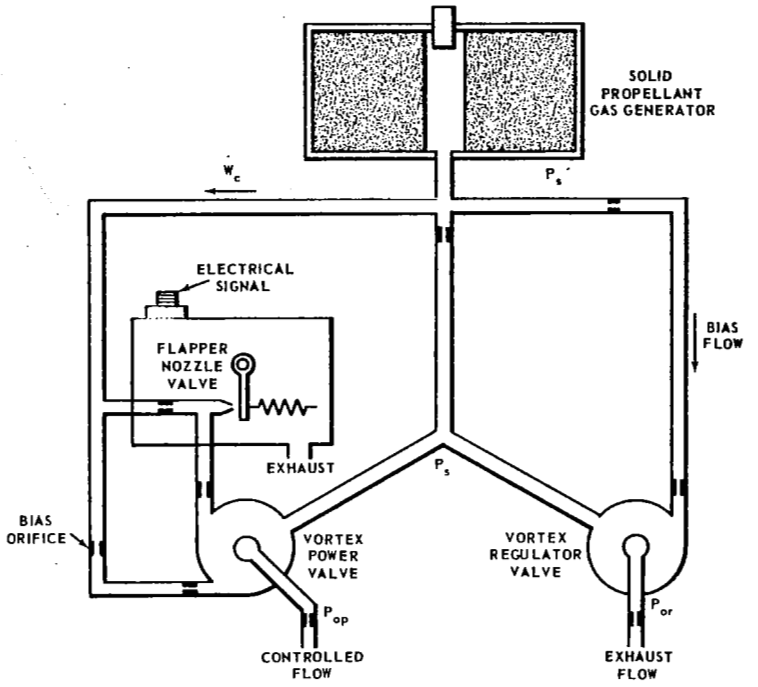

Figure 1 - Basic Circuit Schematic

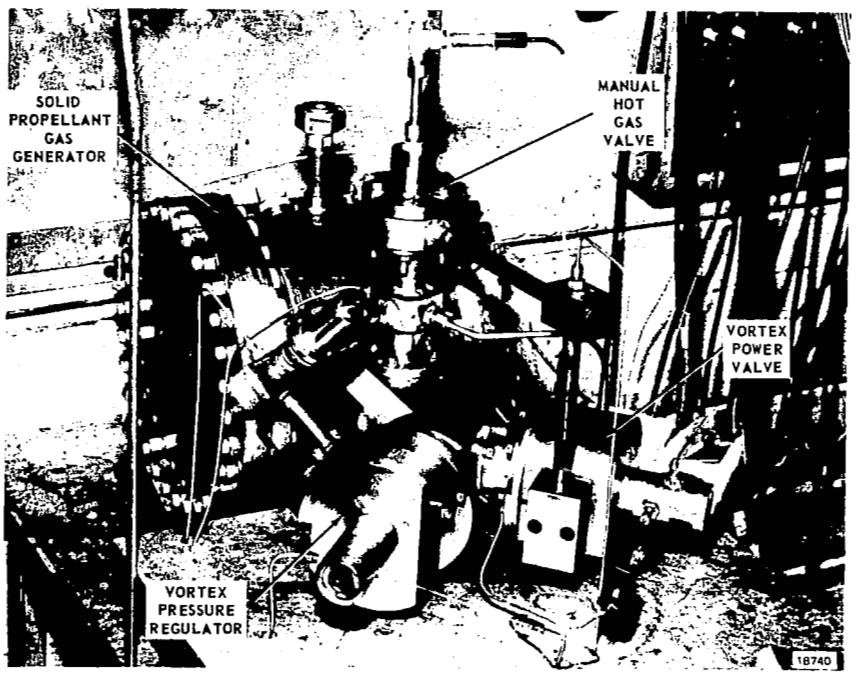

Figure 2 - System Test Installation

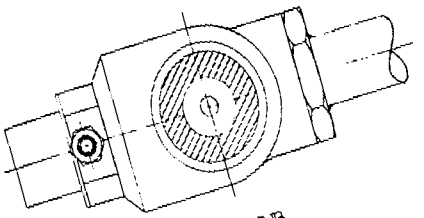

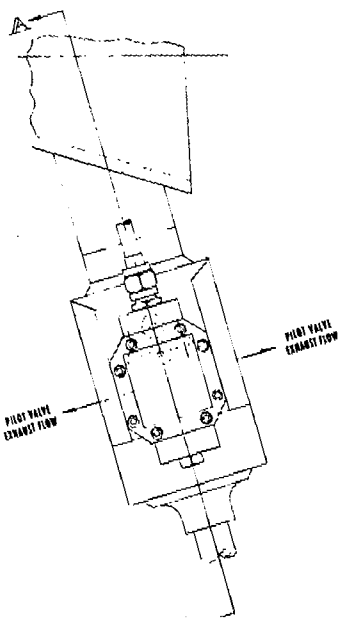

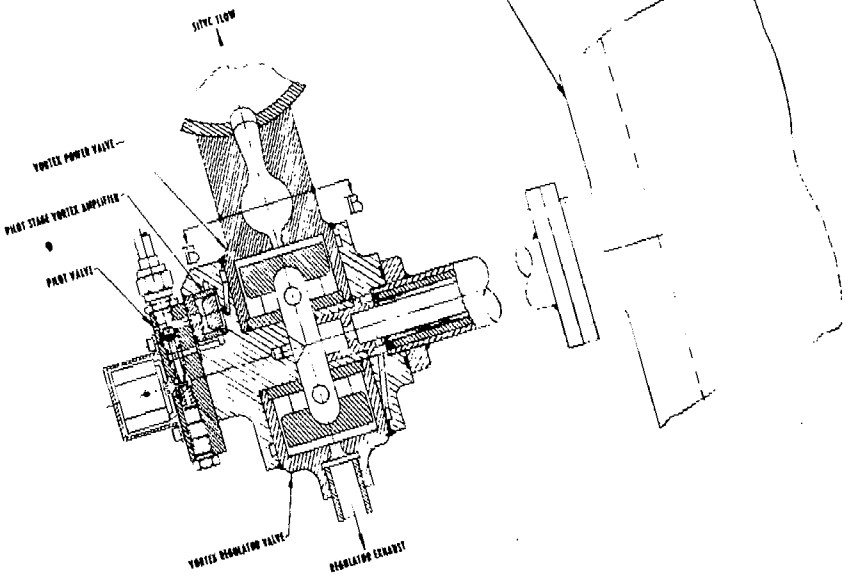

Light-Weight Design of SITVC System

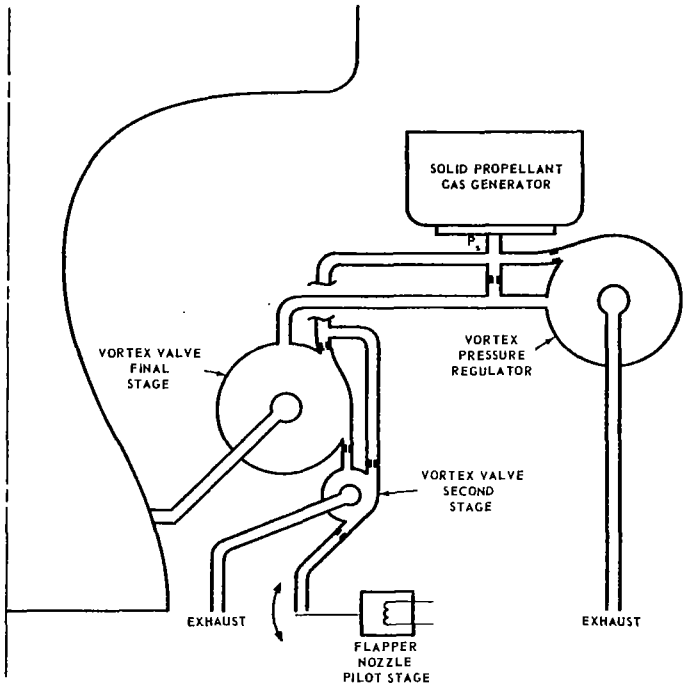

Figure 4 - Staged Vortex Valve SITVC

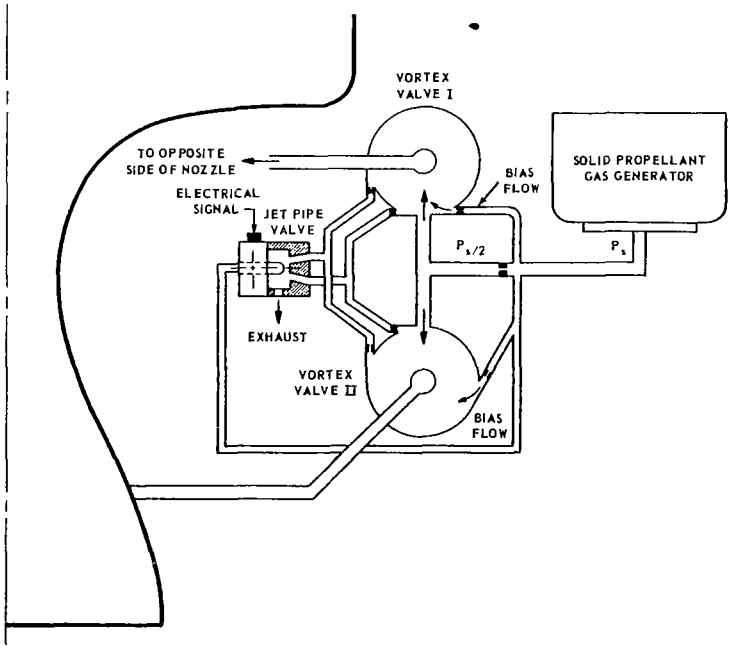

Figure 5 - Push-Pull Vortex Valve Secondary Injection System

push-pull configuration (Figure 5) utilizes control input summing; this was eliminated because of complexity.

The goal was to choose a system that is most representative and provides maximum information on performance, enabling final choice of the best system configuration.

Performance Analysis

A steady state analysis was conducted to determine pressures and flows throughout the system. The analysis was accomplished to interface the system components for best performance. This analysis is summarized in Appendix A. Significant system performance relationships for the vortex power valve and vortex regulator valve are shown in Table 1. These relationships are used to design the complete system. All the system parameters required for design are summarized in Table 2.

An important consideration is the correlation of performance when operating with cold gas and hot gas. This can be compared by evaluating the flow through an orifice using pressure ratios for correlation. The flow through an orifice is calculated by the relationship:

$$\dot{W} = C\, C_d\, A\, \frac{P_u}{\sqrt{T_u}}\, f_1\left(\frac{P_d}{P_u}\right) \qquad (1)$$

where:

C = constant dependent on thermodynamic gas properties

C_d = orifice coefficient, assumed constant and equal for hot or cold gas

A = orifice area

P_u = upstream pressure

T_u = upstream stagnation temperature

P_d = downstream static pressure

f_1 = orifice flow function, dependent on thermodynamic properties.

The coefficients C and f_1 can be evaluated using the equations contained in Appendix A.

Table 1 - Vortex Valve Pressure and Flow Relationship

	Regulator Valve	Power Valve
Max. Control Pressure to Supply Pressure Ratio, P_c/P_s	1.08	1.23
Max. Valve Control Flow to Total System Flow Ratio, $\dot{W}_c/\dot{W}_o$	0.176	0.196
Max. Valve Outlet Pressure to Supply Pressure Ratio, P_o/P_s	0.2	0.51

Table 2 - System Design Parameters

Parameter	Hot Gas	Cold Gas
P_s	2250	2250
P_{br}	1840	1840
P_c(nom.)	1900	1900
P_s(nom.)	1750	1750
P_{op}(max.)	950	950
P_{or}(max.)	425	425
$\dot{W}_s$	1.04	2.86
$\dot{W}_{br}$	0.144	0.396
$\dot{W}_c$	0.163	0.446
$\dot{W}_s$	0.896	2.46
$\dot{W}_{or}$(max.)	0.817	2.24
$\dot{W}_{op}2$(max.)	0.83	2.38

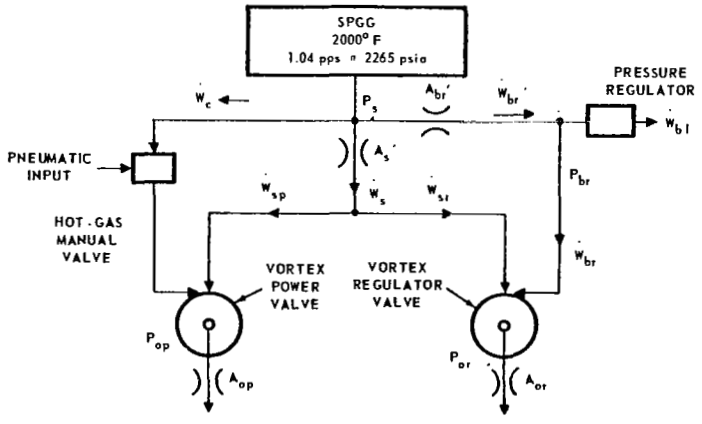

$$f_1\left(\frac{P_d}{P_u}\right) = 1 \text{ (for sonic flow conditions)}$$

C for N_2 = 0.523 $°R^{1/2}$/sec

C for OMAX 453D solid propellant = 0.412 $°R^{1/2}$/sec

Rearranging equation (1):

$$\frac{\dot{W}\sqrt{T_u}}{C} = C_d A P_u$$

The value of $C_d A P_u$ does not depend on thermodynamic properties. Therefore, the equivalent nitrogen flow passing through an orifice designed for hot-gas flow using the same upstream pressure can be calculated using the following expression:

$$\dot{W}_{OMAX} = \dot{W}_{N_2}\left(\frac{0.412}{0.523}\right)\left(\frac{530}{2460}\right)^{1/2}$$

thus:

$$\dot{W}_{OMAX} = 0.365\ \dot{W}_{N_2}$$

An important consideration in system design is minimizing erosion and heat loss in the manifolding. The flow Mach number was always kept below 0.15. The relationship for assuring this is:

$$A = 417\frac{\dot{W}}{P}$$

where:

A = cross sectional area of the tube ($in.^2$)

$\dot{W}$ = weight flow rate (lb/sec)

P = local pressure ($lb/in.^2$)

A dynamic analysis of the basic system shown in Figure 1 was performed and is included as Appendix B. This analysis was made to determine the effect of the manifold volumes on the system performance. Testing accomplished with the vortex valve has shown its response to be approximately an order of magnitude faster than that of the associated control and supply volumes; therefore, it is not included in complete system analysis. In addition, the dynamics of the supply source were not considered in the analysis. This allows some error when comparing between cold- and hot-gas tests. Figure 6 is the block

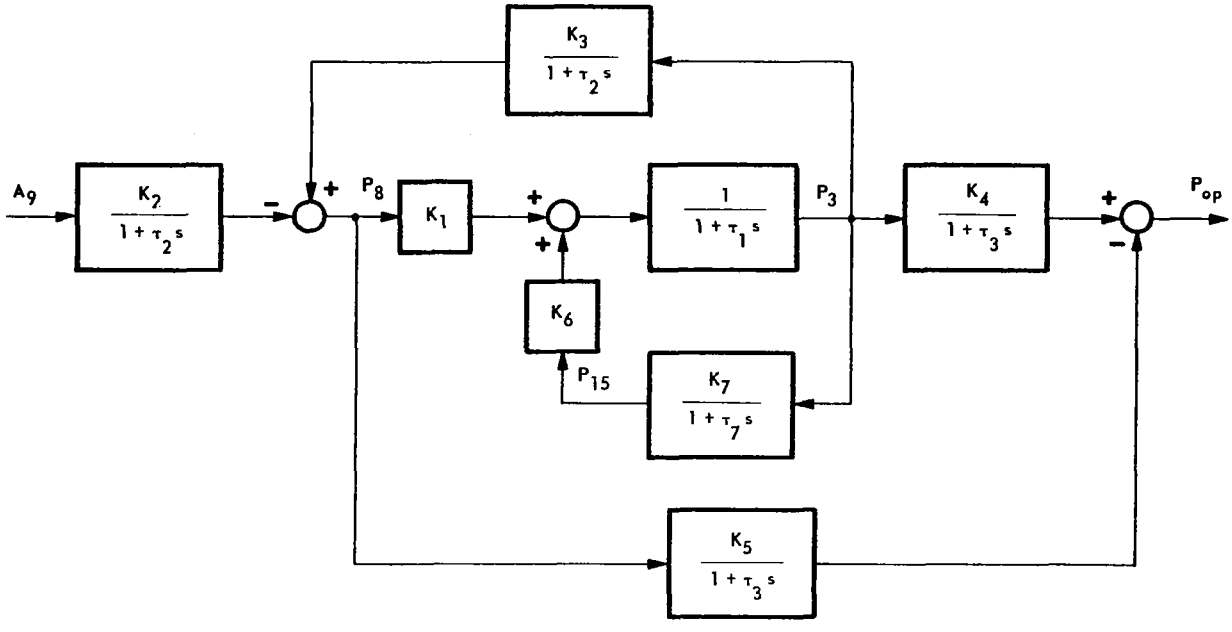

Figure 6 - System Block Diagram

diagram of the basic system shown in Figure 1. The complete system transfer function is:

$$\frac{P_{op}(s)}{A_9(s)} = -\left\{ \frac{K_1 K_4 (1+\tau_7 s)(K_4 - K_3 K_5 + K_4 \tau_2 s)}{K_1 K_3 K_4 (1+\tau_3 s)(1+\tau_7 s) + K_4 (1+\tau_2 s)(1+\tau_3 s)\left[-K_6 K_7 (1+\tau_1 s)(1+\tau_7 s)\right]} - \frac{K_5}{1+\tau_3 s} \right\} \frac{K_2}{1+\tau_2 s}$$

Figure 7 is a Bode plot of this transfer function. The system can also be approximated by a single order system expressed as:

$$\frac{P_{op}(s)}{A_9(s)} = \frac{K}{1+\tau_1 s}$$

where:

$$\tau = \frac{1}{713} \text{ for } 2000°F \text{ gas (0MAX 453D propellant)}$$

If the time constant is related to the predominant system volume under compression and gas properties, then the expression for τ_1 is:

$$\tau_1 = \frac{PV}{kRT\dot{W}}$$

$$(1)\quad \frac{P_{op}(s)}{A_9(s)} = \left\{ \frac{K_1 K_4 (1+\tau_7 s)(K_4 - K_3 K_5 + K_4 \tau_2 s)}{K_1 K_3 K_4 (1+\tau_3 s)(1+\tau_7 s) + K_4 (1+\tau_2 s)(1+\tau_3 s)\left[-K_6 K_7 (1+\tau_1 s)(1+\tau_7 s)\right]} - \frac{K_5}{1+\tau_3 s} \right\} \frac{K_2}{1+\tau_2 s}$$

$$(2)\quad \frac{P_{op}(s)}{A_9(s)} \approx \frac{1}{\left(1+\frac{s}{732}\right)} \qquad \text{HOT GAS APPROXIMATION}$$

$$(3)\quad \frac{P_{op}(s)}{A_9(s)} \approx \frac{1}{\left(1+\frac{s}{311}\right)} \qquad \text{COLD GAS APPROXIMATION}$$

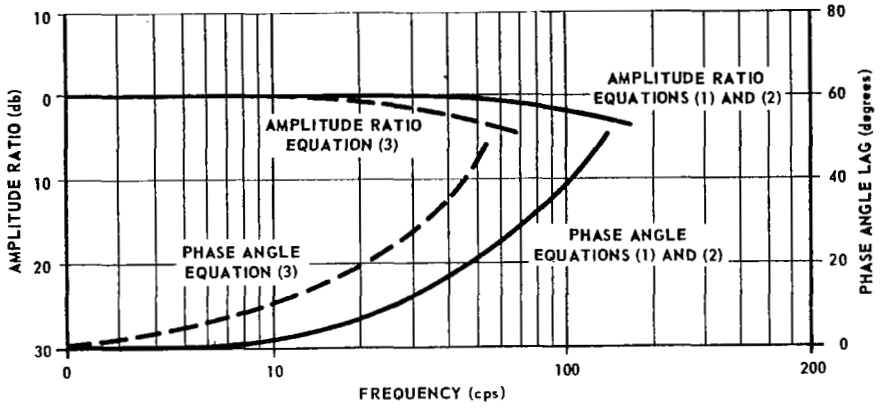

Figure 7 - System Frequency Response - Predicted

To determine the equivalent time constant for operation with cold gas, variables for an equivalent volume and pressure are equated:

$$P V = \tau k R T \dot{W}$$

The dynamic response is dependent only on the gas properties. Thus:

$$\tau k R T \dot{W} \text{ (cold)} = \tau k R T \dot{W} \text{ (hot)}$$

Substitution of the thermodynamic gas properties yields:

$$\tau \text{ (cold)} = 2.4\ \tau \text{(hot)}$$

Using the approximate transfer function for evaluation of cold-gas dynamic performance results in:

$$\frac{P_{op}(s)}{A_9(s)} \approx \frac{K}{1+\frac{s}{314}}$$

This is also plotted in Figure 7 for comparison with hot-gas performance.

Thermal Analysis

A simplified thermal analysis was accomplished to determine the adequacy of the insulation used throughout the system. The analysis did not include changes in the film coefficients due to outgassing of the phenolic or the change in thermal conductivity due to char. Based on previous experience, the calculated temperature is usually found to be slightly higher than the actual value. The highest temperature which could be tolerated on the back side of the insulation was 500°F.

Erosion in the supply manifold, where the supply flow changed direction, was eliminated by increasing the area to reduce the gas velocity. Insulation was redesigned after the first test because the asbestos-phenolic insulation sloughed and plugged the valves. A composite structure of high density graphite and asbestos-phenolic was incorporated, and this functioned satisfactorily.

A dual seal technique was used for flange type joints. Flat gasket insulators made of asbestos-phenolic minimized heat transfer. Viton O-rings were used for static seals in these areas. Where insulation could not be provided, copper crush rings were used. The copper rings were retained in serrated cavities. Seals were kept to a minimum by utilizing welded assemblies whereever possible.

Sealing the vortex valve control orifices required that the orifice be made with a pilot diameter and a conical sealing face seated on a sharp edge in the housing. The orifice pilot diameter fitted into the housing with a slip fit so that thermal expansion of the orifice provided an additional sealing surface in case the conical sharp edge seal failed. The orifice was loaded into the housing using a compression nut.

SYSTEM DESIGN

The system design philosophy was based on flexibility. Heavyweight hardware was utilized to allow modifications to be incorporated as needed. All of the vortex valve components were made for easy replacement, allowing substitution of parts for configuration modification. One of the primary requirements was to insulate the gas generator and manifold to assure delivery of 2000°F gas to the vortex valves. In addition, close coupling between the generator and valves was required to minimize heat loss. All materials were selected to eliminate erosion and to allow several firings with the same system.

Vortex Regulator and Power Valve

The internal configuration of the vortex regulator and power valve are similar except for the control flow injector size and difference in chamber geometry to provide desired gain characteristics. A layout drawing of the prototype system (Figure 8) shows the design of the vortex regulator and power valve.. This is a heavyweight design to allow flexibility in modification and permit several test firings on the same hardware. The hot-gas generator and manifold supplying hot gas are completely insulated to assure delivery of hot gas to the valves at the maximum gas temperature throughout the operating duration.

The button and chamber housing of each valve are made from 300 series stainless steel. These parts are rough machined, stress relieved, and finish ground to final dimensions. The vortex chamber is sealed to the manifold mounting flange, using Viton O-rings.

The chamber outlet orifice is made from an alloy of molybdenum (Mo - 0.5 Ti). It is inserted into a pilot diameter of the vortex chamber housing using a slip fit. The slip fit provides a chamber seal during a hot firing by relative thermal expansion. The orifice is held in place by a retaining nut. The nut forces the orifice conical surface against the chamber seat, providing an additional seal.

A plenum chamber is located at the vortex valve outlet which includes an orifice at the outlet for simulating the secondary injection flow nozzle. This provides the means for measuring the outlet flow during a hot firing. The plenum chamber pressure can be directly correlated with flow through the load orifice. The plenum is fabricated from stainless steel and is sealed to the vortex chamber housing using a flat copper crush gasket.

The control flow injectors for the vortex valves are rough machined from an alloy of molybdenum (Mo - 0.5 Ti). They are then stabilized at 2000°F for one hour in an inert atmosphere. This produces a grain structure which minimizes

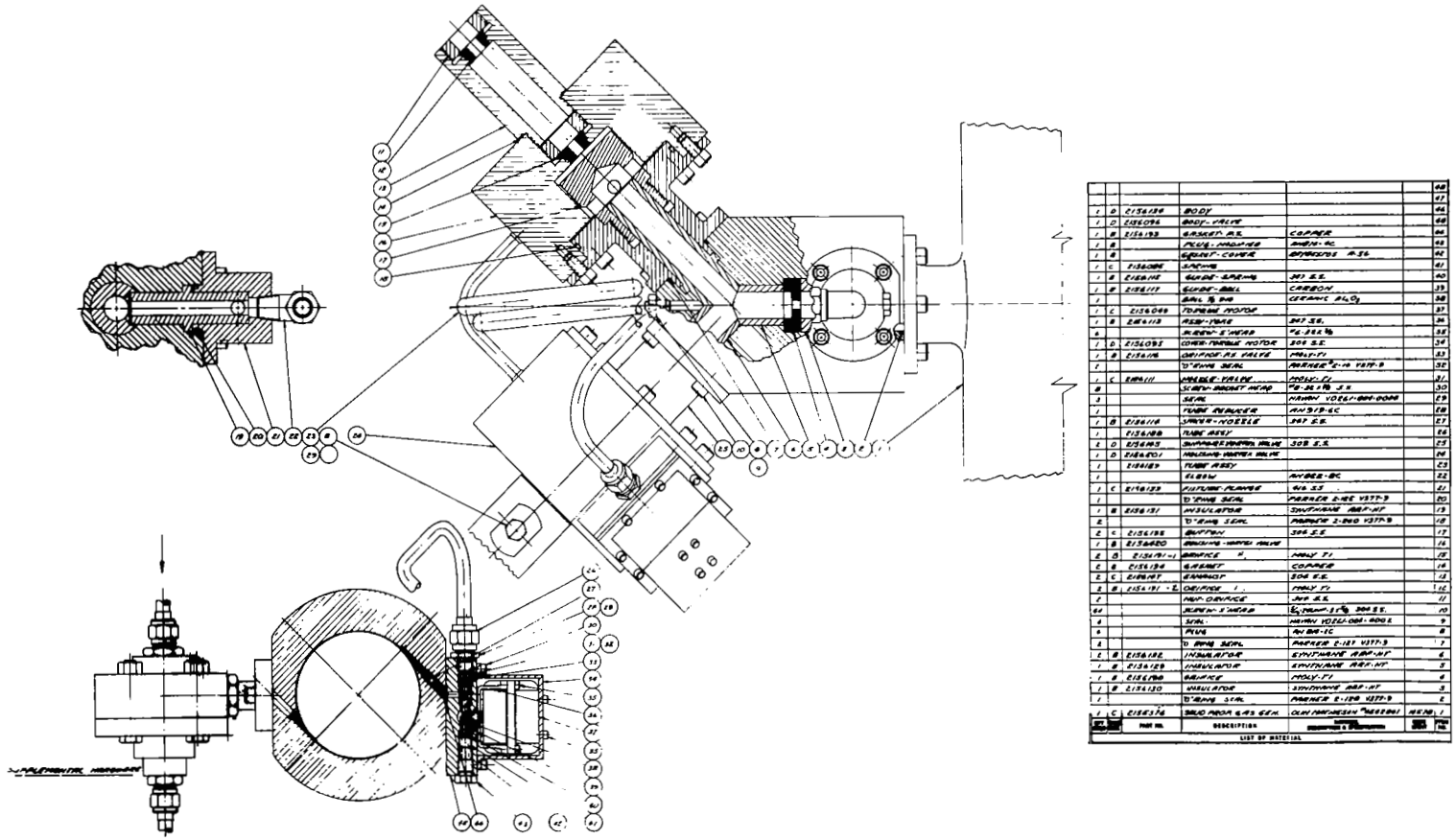

Figure 8 - 2000°F SITVC System, Assembly Drawing

erosion. The injectors are installed in the vortex chamber housing with a press fit, and the protruding end is finish ground flush with the bore. The same injectors were used for all five hot-gas system tests with no noticeable erosion or expansion loosening.

The vortex regulator and power valve differ primarily in size of control flow injectors. The vortex regulator injection area is 0.0173 $in.^2$. The power valve injection area is 0.0117 $in.^2$. The larger regulator valve area increases the valve gain, which is reflected in a lower control pressure required for full flow modulation.

The valves tested had different vortex chamber diameter ratios. The regulator valve had a ratio of chamber diameter to outlet hole diameter of 6 to 1. The power valve had a ratio of 10 to 1. Based on limited testing, it was originally estimated that the relative diameter ratios were required for achieving the desired gain characteristics. Testing to date, however, indicates the power valve diameter ratio can be decreased to 6 to 1 without degrading performance. This has been extensively evaluated in other development programs.

A summary of significant design parameters is shown in Table 3. The general design of the vortex valve is extremely simple because no moving parts are required. This extreme simplicity minimizes design and fabrication problems.

Pilot Stage Valve

Design tradeoffs for selecting the pilot-stage valve configuration indicated that the flapper-nozzle design was best suited for this application. It has the least number of moving parts and is especially compatible with the high system pressure. (Conventionally the flapper-nozzle valve is operated push-pull as shown in Figure 9). This system application required only a single flow to the vortex power valve. To balance the pressure force of the nozzle on the flapper, one side of the flapper has a balanced spring load as shown in Figure 10. Photographs of the assembled valve and an exploded view are shown in Figures 11 and 12.

The spring load is transmitted to the flapper through a stainless steel plunger and ceramic ball. The ball contacts the flapper and provides a thermal barrier between the plunger, spring, and flapper, thus minimizing heat conduction to the spring. The plunger and ball slide inside a carbon insert guide which insures correct alignment between the spring load and the flapper. To set a desired control pressure, the spring load is adjusted to provide a balanced load on the flapper at zero differential current. This eliminated the need for a torque motor holding current to attain the necessary flapper null position.

This single-sided valve can be easily modified to provide another controlled flow without changing the valve geometry or affecting the primary output. This

Table 3 - Breadboard Vortex Valve Design Parameters

	Power Valve	Regulator Valve
D_s (in.)	0.167	0.172
L (in.)	0.105	0.063
D_{ch} (in.)	1.64	0.984
A_c (in^2)	0.00238	0.00915
K (in.)	0	0
A_a (in^2)	0.225	0.089
A_o (in^2)	0.043	0.043

Note: See Figure 20 for identification of dimensions.

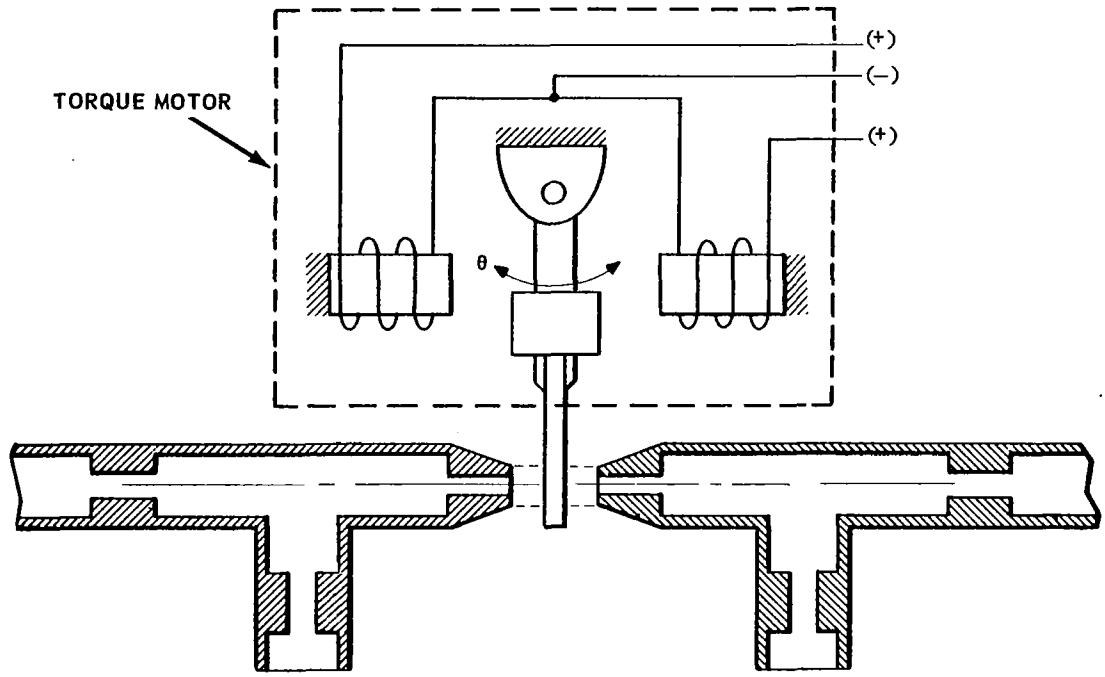

Figure 9 - Conventional Flapper-Nozzle Pilot Valve

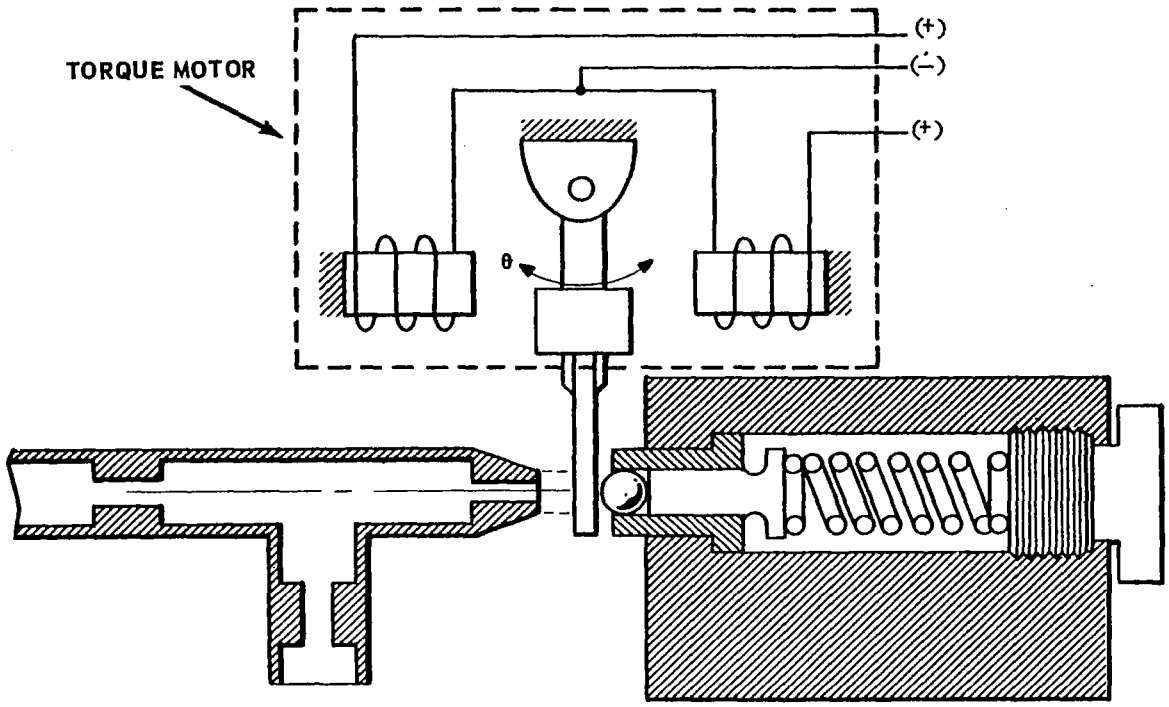

Figure 10 - Flapper-Nozzle Pilot Valve with a Single Output

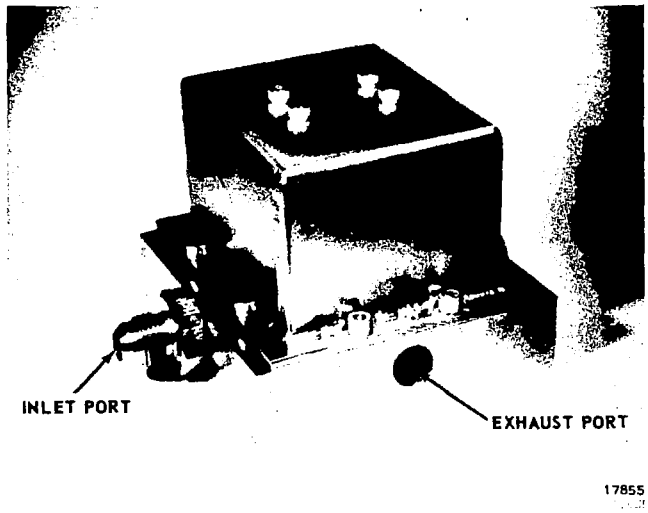

Figure 11 - Flapper-Nozzle Valve - Assembled View

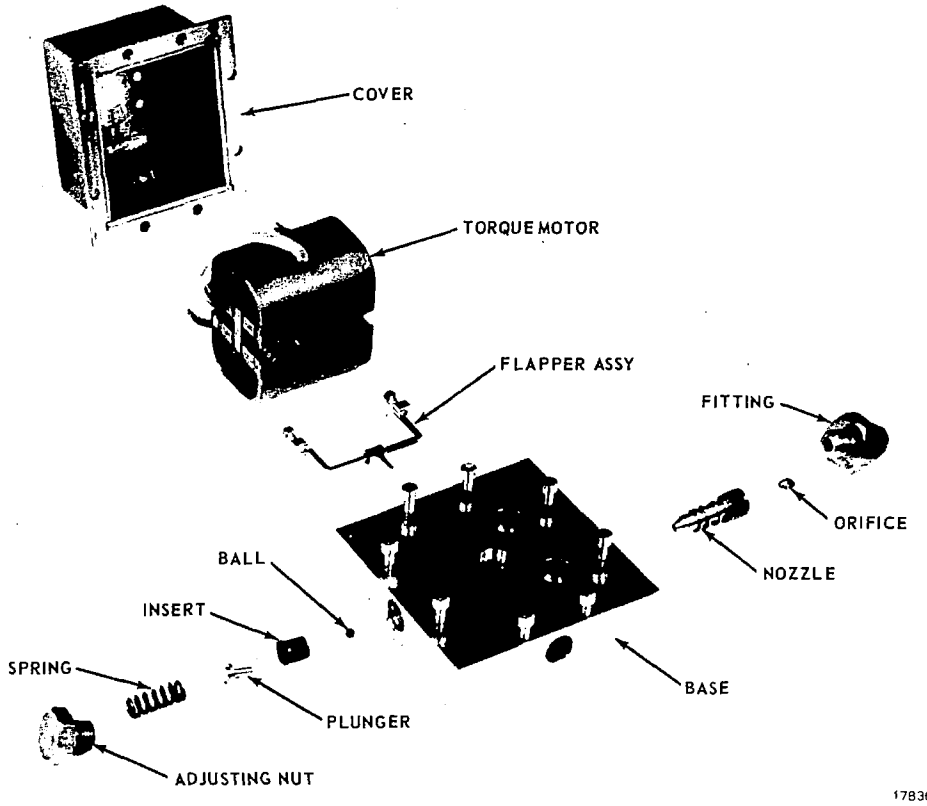

Figure 12 - Flapper-Nozzle Valve - Exploded View

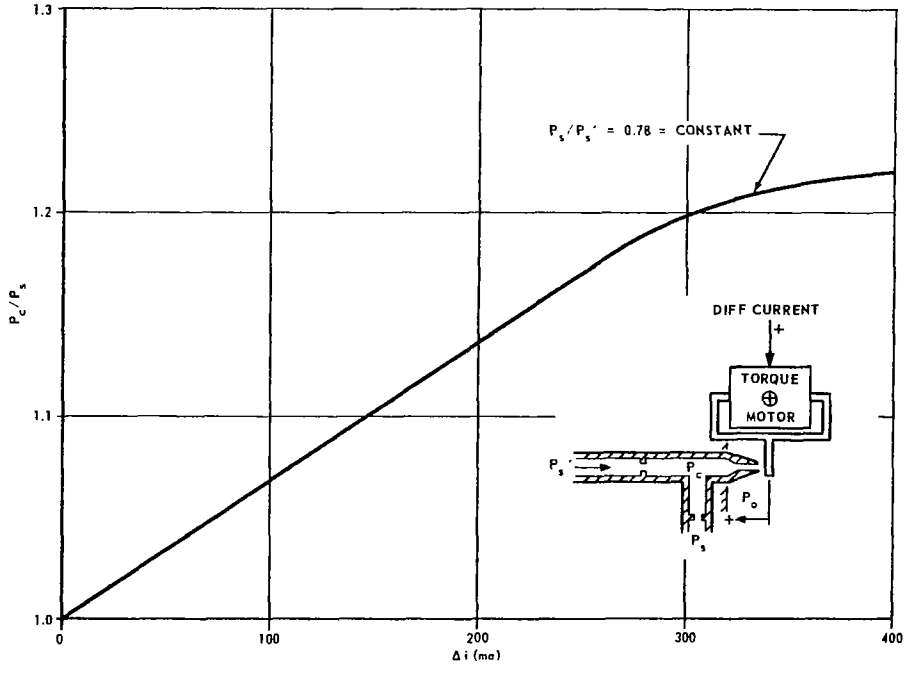

Figure 13 - Pilot Valve Cold-Gas Static Performance

is accomplished by substituting a nozzle and pressure dropping orifice for the spring restraining assembly. The second output could be used in conjunction with another vortex power valve for controlling a push-pull system.

The torque motor, which drives the flapper, is a standard Servotronics Model 20-4 with minor mounting modifications. Thermal isolation is achieved by minimizing the conducting surface area. This prevents the torque motor temperature from exceeding 400°F.

A 300 series stainless steel was selected for the base and torque motor cover because it is non-magnetic and has adequate elevated temperature mechanical properties. These parts were rough machined and stress relieved prior to final machining. This eliminated possible distortion during initial firings.

The nozzle, orifice, and flapper were made from an alloy of molybdenum (M0 - 0.5 Ti). It has a low coefficient of thermal expansion and a high specific heat which makes it an ideal material for this application. This material withstood three repeated firings before requiring replacement. The material selected for the flapper yoke was Rene 41, a high-temperature alloy commonly used for jet engine turbine vanes and shrouds.

Cold- and hot-gas tests were conducted to determine the pilot valve performance. Figure 13 is the static performance plot of control pressure (P_c) versus differential current. Figure 14 shows the dynamic performance using cold gas for the same valve configuration. The flapper was stroked to 70 percent of full stroke against a nominal back pressure of 1050 psia during the cold-gas test. Although frequency response data was taken to 400 cps, the input signal became distorted beyond 200 cps. Data beyond this point should not be used. The plot shows an amplitude attentuation of -1.2 db at 100 cps and a phase shift of 55 degrees. The amplitude attenuation compares very favorably with the analysis. The predicted break frequency was 95 cps.

The hot-gas frequency response test was conducted on the pilot valve just prior to system firing No. 5. Figure 15 shows the pilot valve after a hot-gas test.

Solid Propellant Gas Generator

The SPGG was designed and manufactured by Olin Mathieson to supply the SITVC system with 2000°F hot gas. Although the SPGG breech is a special design, the grain formulation is standard Olin "OMAX 453D" which is fully developed and qualified. The SPGG design is shown in Figure 16.

The generator consists of an ignitor, a breech, two solid propellant ammonium nitrate grains, insulation, and a burst diaphram assembly. A flange-type outlet, incorporating a cylindrical throat insulation insert, is provided. The flange outlet mounts to the SITVC system and is sealed with a Viton O-ring. The insulation prevents localized heating of the outlet fitting.

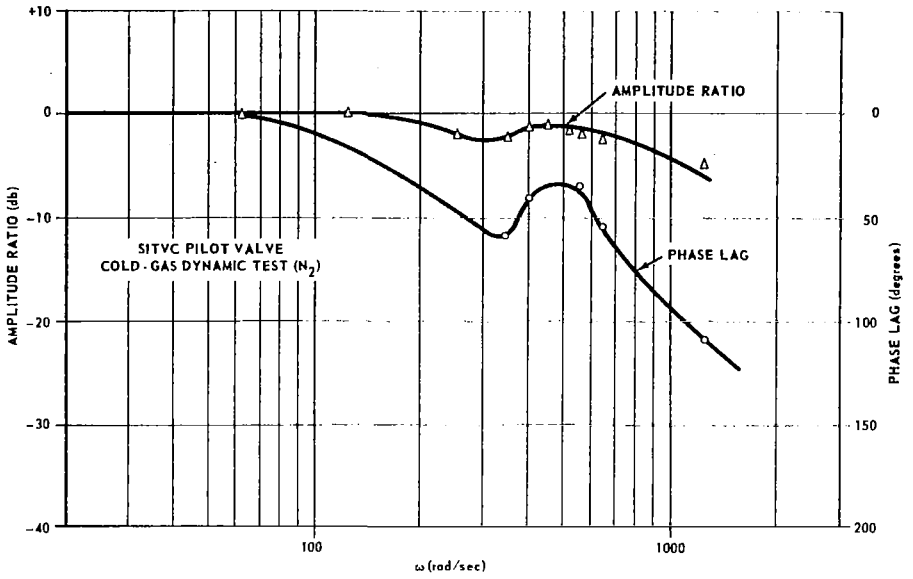

Figure 14 - Pilot Valve Cold-Gas Dynamic Performance

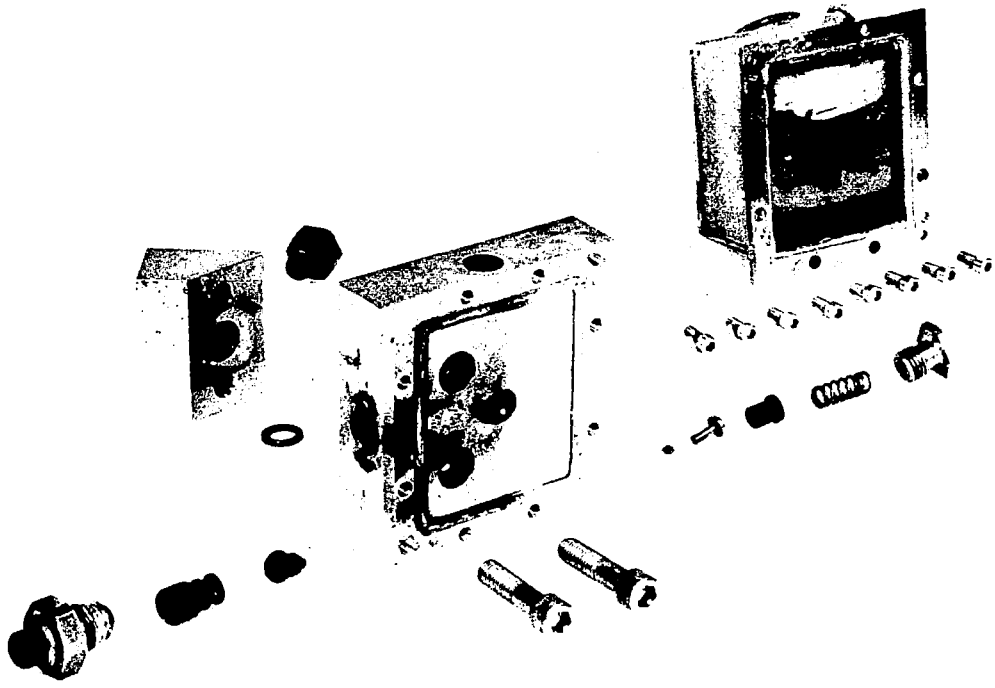

Figure 15 - Pilot Valve after Hot-Gas Test

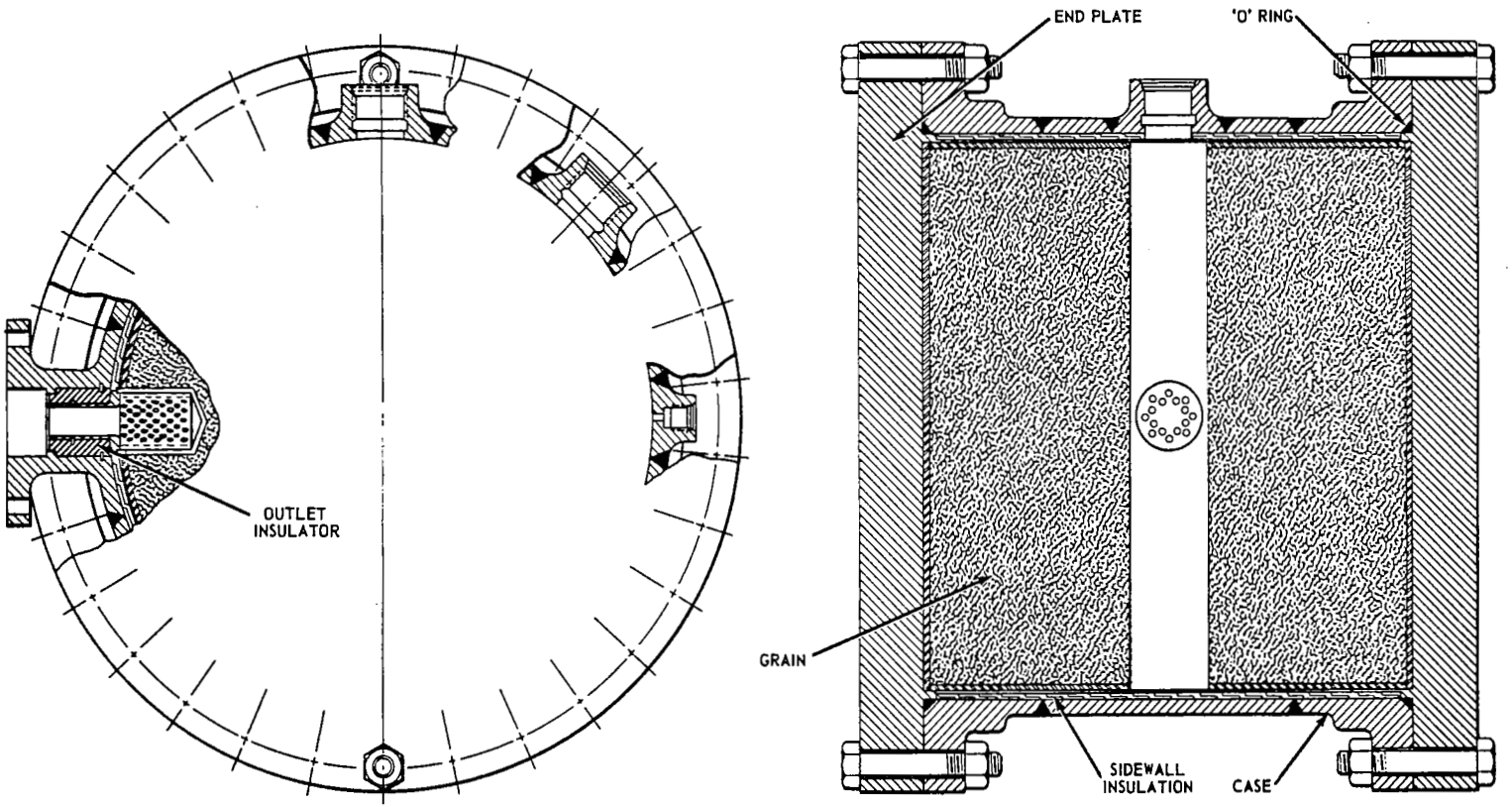

Figure 16 - Solid Propellant Gas Generator

The ignitor, made by Holex, is a dual-bridge type designed for a 0.5 ampere no-fire current and 3 ampere sure fire. This is a reliable unit qualified to military specifications. It is retained in the breech casing in an AND port and sealed with a Viton O-ring.

The breech assembly, consisting of the case and end caps, is made from 4130 steel, heat treated to a tensile strength of 180,000 psi. This material was selected for its good welding properties and high tensile strength. The end caps are secured to the breech with 32 high-strength bolts. Crush type Viton O-rings are used to seal the end caps and casing. The casing and outlet fittings are well insulated to prevent local hot spots. During hot-gas tests, case soakback temperatures have not exceeded 200°F. The heat shield inside the breech retains the booster charge in a fixed position relative to the ignitor. The outlet insulation and dirt screen index the heat shield and casing insulation to the case. The outlet and pressure instrumentation ports were welded to the case prior to heat treating.

The breech contains two solid propellant ammonium nitrate end-burning grains which burn concurrently, producing a gas weight flow of 1.04 lb/sec at 2290 psi pressure with a flame temperature of 2000°F. These grains have neutral burning characteristics. The results of a hot-gas ballistic test on the SPGG are shown in Figure 17.

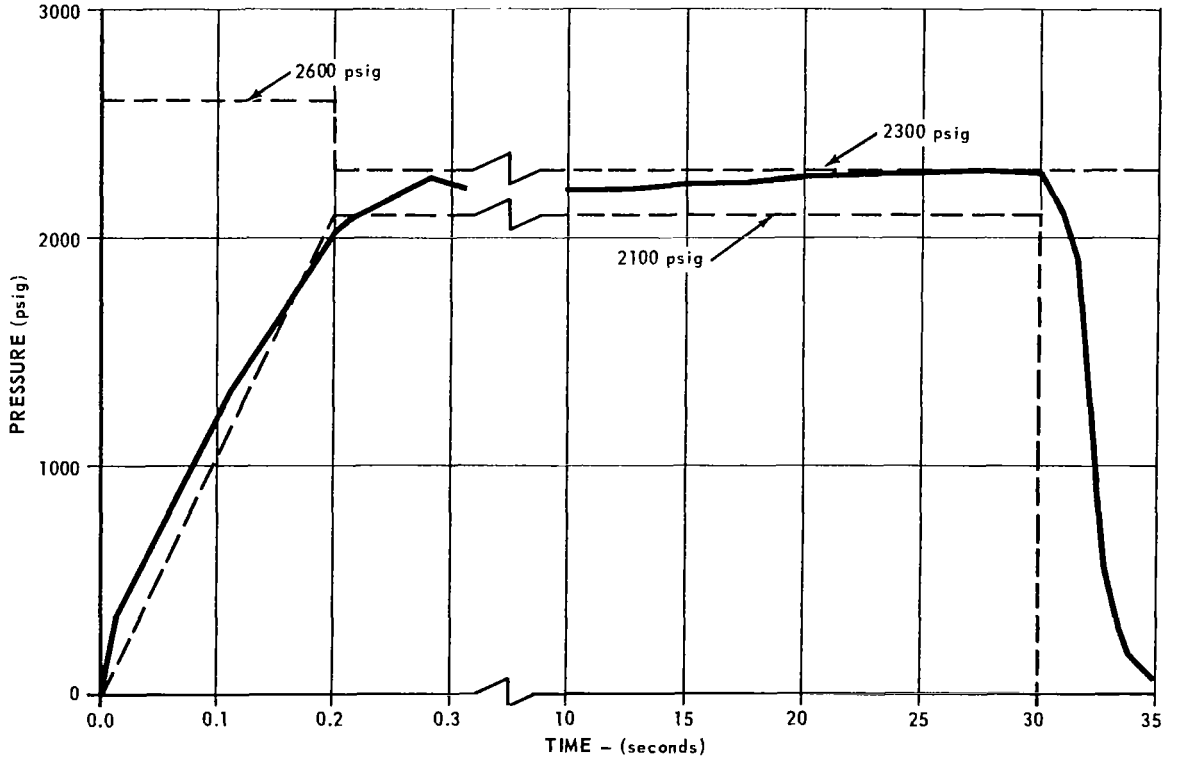

Figure 17 - Ballistics Data SPGG

Although the SPGG showed satisfactory ballistic performance, the breech failed to meet the specified proof pressure test. Since this was an acceptance requirement, the schedule was delayed considerably for redesign and rework before a final unit was delivered which was suitable for system testing.

SYSTEM TEST AND EVALUATION

The development of the vortex valve secondary injection control system was accomplished in three steps. (1) An extensive cold-gas scale model test and performance optimization study was performed to provide the desired valving characteristics for the vortex power valve and vortex regulator valve. (2) The prototype hardware for hot-gas test was designed and fabricated based on the results of the scale model testing; again cold-gas testing was conducted to optimize performance. Knowledge gained during the scale model test program was used to guide this development. (3) The complete prototype system was assembled and cold- and hot-gas tested.

Breadboard Scale Model Cold-Gas Test

Several breadboard valve models were fabricated and tested to optimize the performance characteristics of the vortex regulator and power valve prior to building prototype full-size units. In particular, it was desired to determine which design parameters influenced valve performance characteristics and to what degree.

An arbitrary valve flow rate was selected for these tests which could be conveniently provided by the high-pressure, low-flow test facilities available. The vortex valves were tested using the schematic shown in Figure 18. This test installation allows convenient variation of flows and pressures and provides flexibility for plotting valve characteristics for changes in control pressure, supply pressure, and output flow. Output flow was correlated with the plenum chamber pressure by flow calibration of the plenum chamber outlet orifice.

Four basic valves were evaluated. Configuration was basically similar, each having two valves with diameter ratios of 10 to 1 and two with diameter ratios of 6 to 1. All the chambers were equipped with four symmetrical control flow injection ports. A button adjustment was provided to allow variation in chamber length. One vortex chamber button of each pair was made larger to evaluate the influence of the annulus over the button on performance. A typical breadboard test model is shown in Figure 19.

Since the control pressure to supply pressure ratio was dictated by system requirements, the parametric tests on the breadboard models were concentrated on evaluating the effects of variations in the vortex chamber length, the size and location of the injection ports, variations in annulus area across the button, and vortex chamber diameter ratio. These significant parameters are shown in a

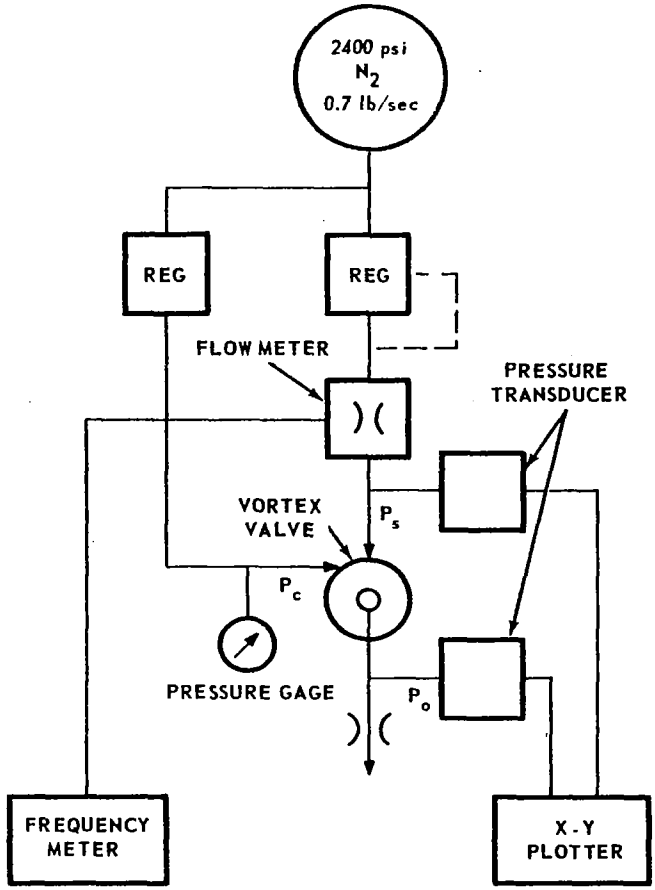

Figure 18 - Vortex Valve Test Schematic

schematic of the vortex valve and plenum chamber (Figure 20). The effect of vortex chamber length on valve performance was evaluated using two valves, one with a diameter ratio of 10 to 1, and the other with a ratio of 6 to 1. All other design dimensions were the same. Both valves showed maximum flow modulation on turndown with a chamber length to vortex chamber outlet hole diameter ratio between 0.5 and 0.125. The valve gain characteristics were dissimilar, which was attributed to the difference in diameter ratio and the annular area between the button and chamber.

The next test series was run to locate the control flow injection point relative to the vortex chamber button. Again two valves with different diameter ratios were evaluated. The control flow injection point was moved axially while all other dimensions were maintained constant. It was determined that the best performance was achieved with the injector center line coinciding with the plane of the button face.

The control flow can be injected in one or several locations. The optimum number was determined by drilling four symmetrical control flow injectors into the valve body; the injectors were not evenly spaced about the chamber periphery

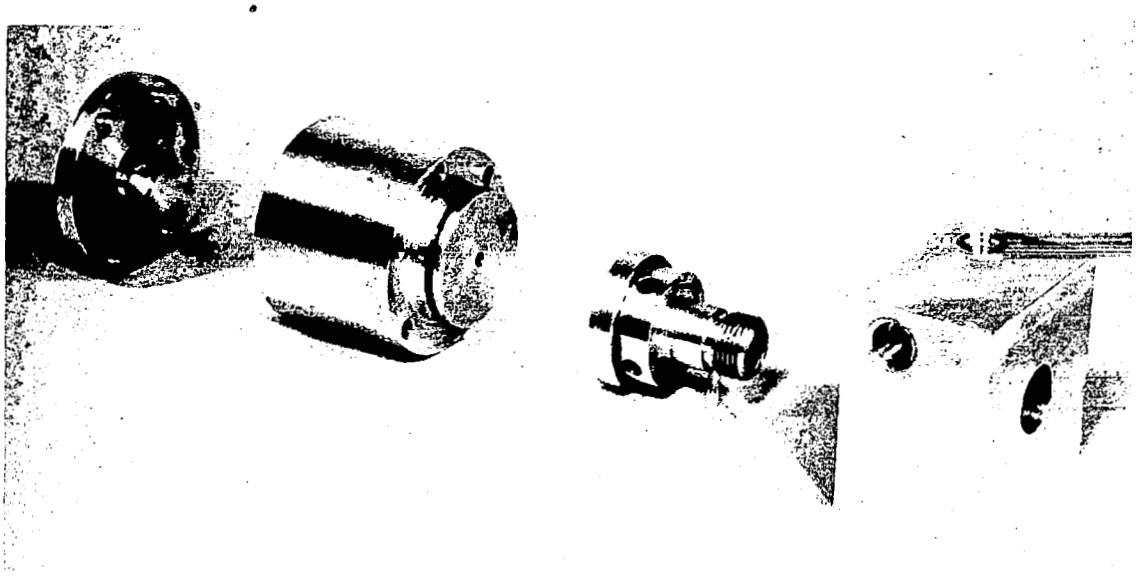

Figure 19 - Vortex Valve - Breadboard Model (1/6 scale)

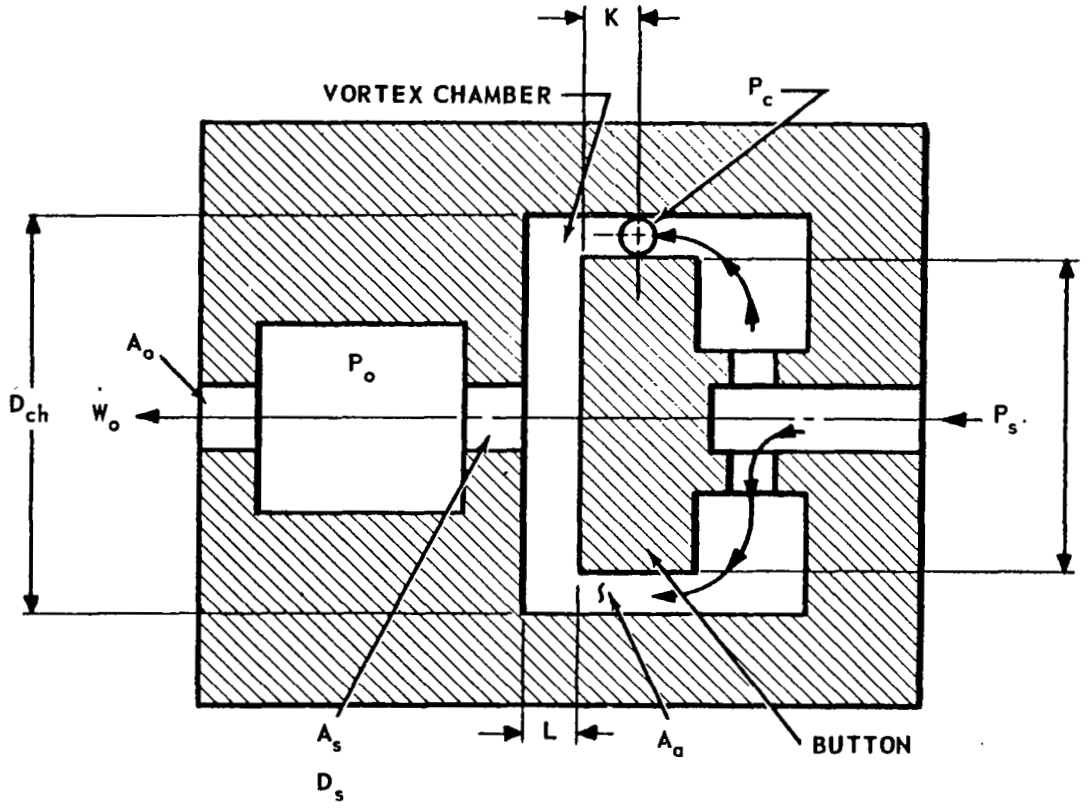

Figure 20 - Vortex Valve - Cross Section Schematic

during this test series. The total injection area equaled 0.125 times the vortex valve outlet area, and this area ratio was preserved throughout the test series. Each test in the series required plugging an injector and opening up the areas of the remaining injectors to maintain the area ratio constant. The test showed the following performance trend: Modulation improves as the number of injectors increases; however, improvement is not significant when more than two injectors are used.

Another variable requiring investigation was the plenum chamber shape. It must be compatible with the vortex valve and nozzle used for SITVC. The plenum chamber has the largest dynamic response time constant, as determined from the dynamic analysis; thus, the frequency response of the system is very dependent on the plenum chamber volume. The vortex valve is not influenced by the plenum chamber size provided that a sonic condition prevails across the valve outlet orifice. Therefore, the chamber was designed for minimum volume and a chamber length that would provide a relatively noise-free chamber pressure reading under steady-state operating conditions. Two chamber configurations were evaluated before these conditions were satisfied.

A typical performance curve for the optimized breadboard power valve is shown in Figure 21. It has a flow modulation range of 5.1 to 1. Optimum power valve vortex chamber geometry is summarized in Table 4.

The optimized performance of the breadboard regulator valve is shown in Figure 22. This valve showed a flow modulation range of 5.48 to 1. Vortex regulator valve geometry is summarized in Table 5.

Prototype Component Cold-Gas Test

The prototype vortex valves were scaled from the breadboard test model, using weight flow as a scaling factor as described in the design section of this report. The final scaled configuration design parameters are summarized in Table 6. Fabricated valves were tested as components using the breadboard valve test techniques described in the preceding section. The general flow relationships scaled very well; the valve gain characteristic changed, however, and maximum flow turndown was not achieved. Valve configuration was modified on the basis of knowledge from the cold-gas breadboard scale model test phase. The final cold-gas performance for the vortex regulator valve is shown in Figure 23. Power valve performance is shown in Figure 24.

A vortex button annulus area to outlet orifice area ratio of 0.418 produced the best valve characteristic for the breadboard power valve. This area ratio represents a radial clearance between the button and housing of 0.035 in. and a radial clearance to injector diameter ratio of 0.69. The same area ratio for the prototype valve resulted in a radial clearance of 0.020 in. with a radial clearance to injector diameter ratio of 0.177. The reduction in button clearance on the pro-

Table 4 - Geometric Relationships

Parameter Ratio	Optimized Value
A_a/A_s	8.27:1
D_{ch}/D_s	8.25:1
L/D_s	0.47
A_s/A_c	11.4
K	0

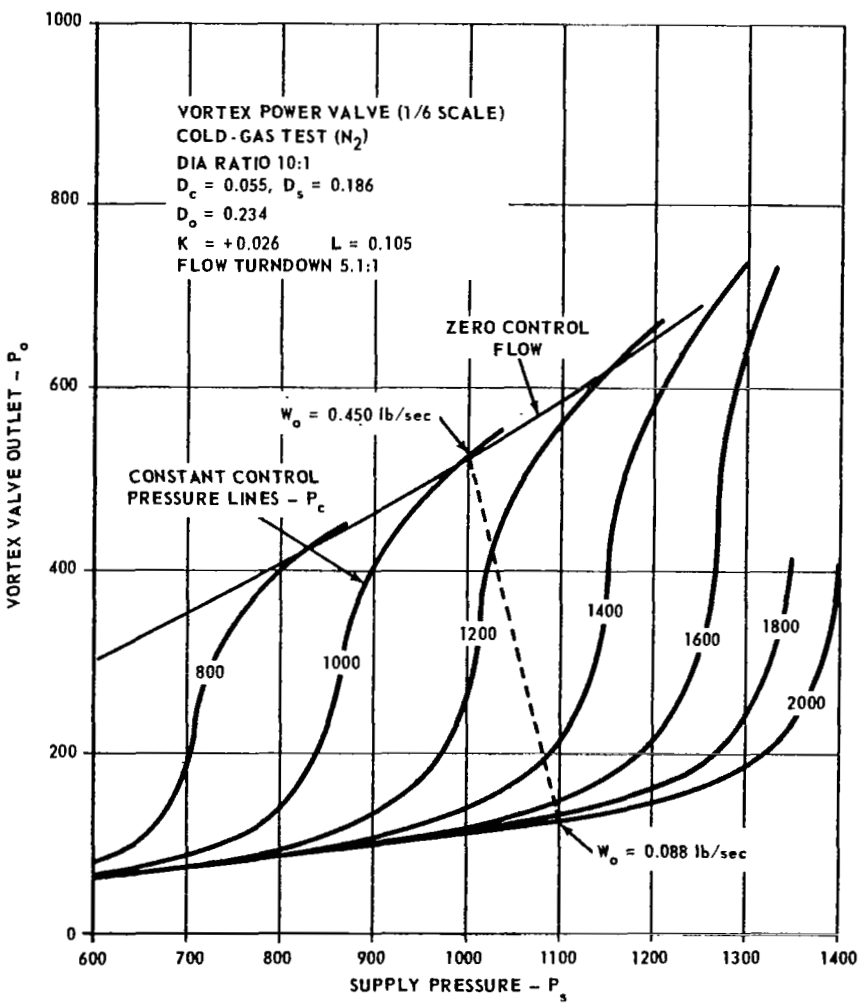

Figure 21 - Vortex Power Valve Flow Gain

Table 5 - Regulator Valve Geometric Relationships

Parameter Ratio	Optimized Valve
A_a/A_s	3.00
D_{ch}/D_s	5.68
L/D_s	0.366
A_s/A_c	7.4
K	0

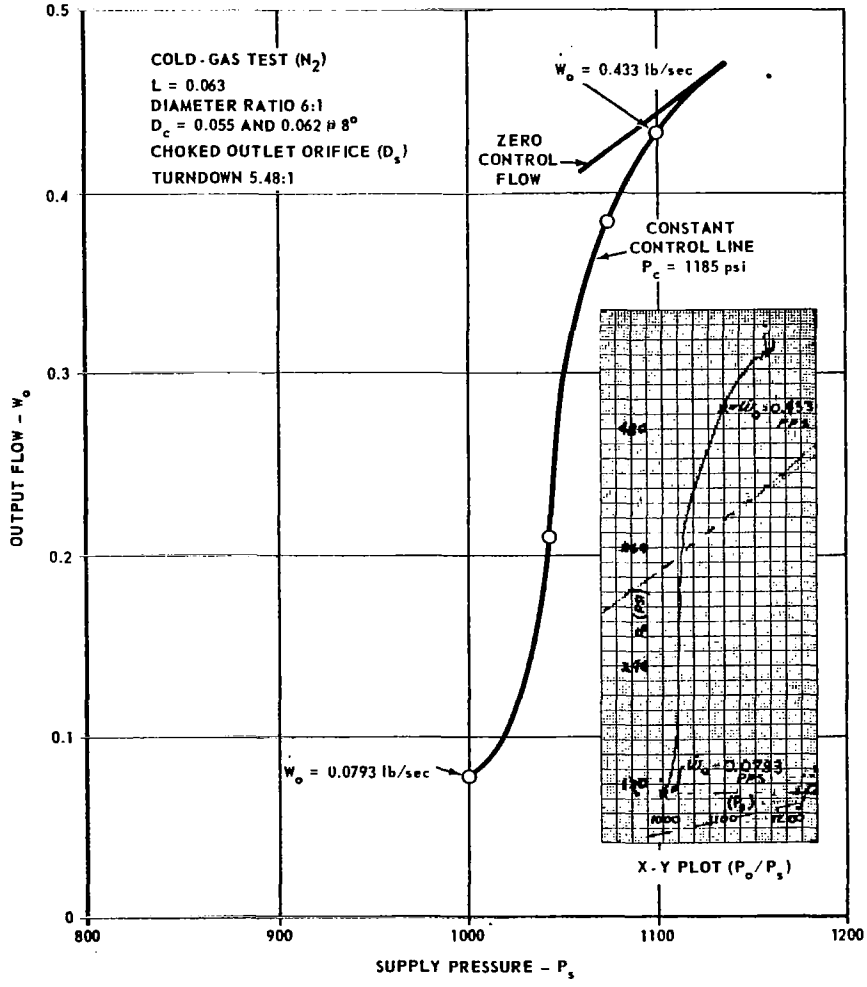

Figure 22 - Breadboard Pressure Regulator - Cold-Gas Test

Table 6 - Prototype Vortex Valve Design Parameters

	Power Valve	Regulator Valve
D_s (in.)	0.272	0.261
L (in.)	0.149	0.105
D_{ch} (in.)	3.62	2.225
A_c (in^2)	0.0117	0.0173
K (in.)	0.049	0.093
A_a (in^2)	0.4126	0.361
A_o (in^2)	0.100	0.217

Note: See Figure 20 for identification of dimensions.

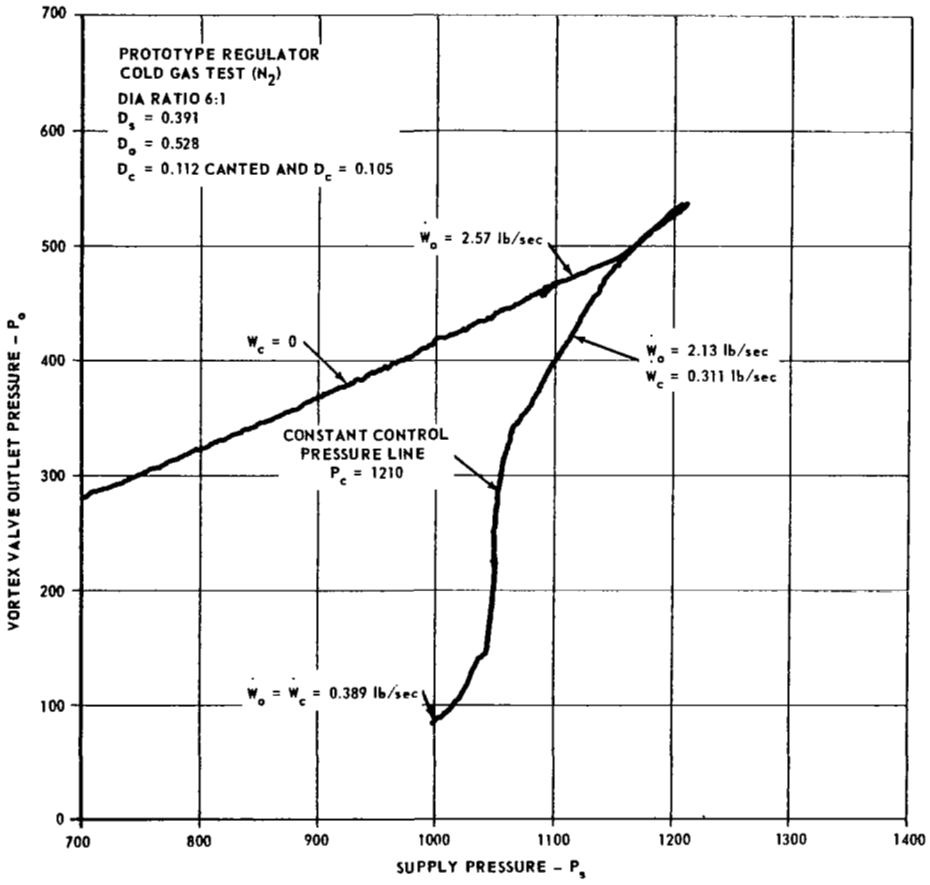

Figure 23 - Prototype Regulator Valve - Cold-Gas Test

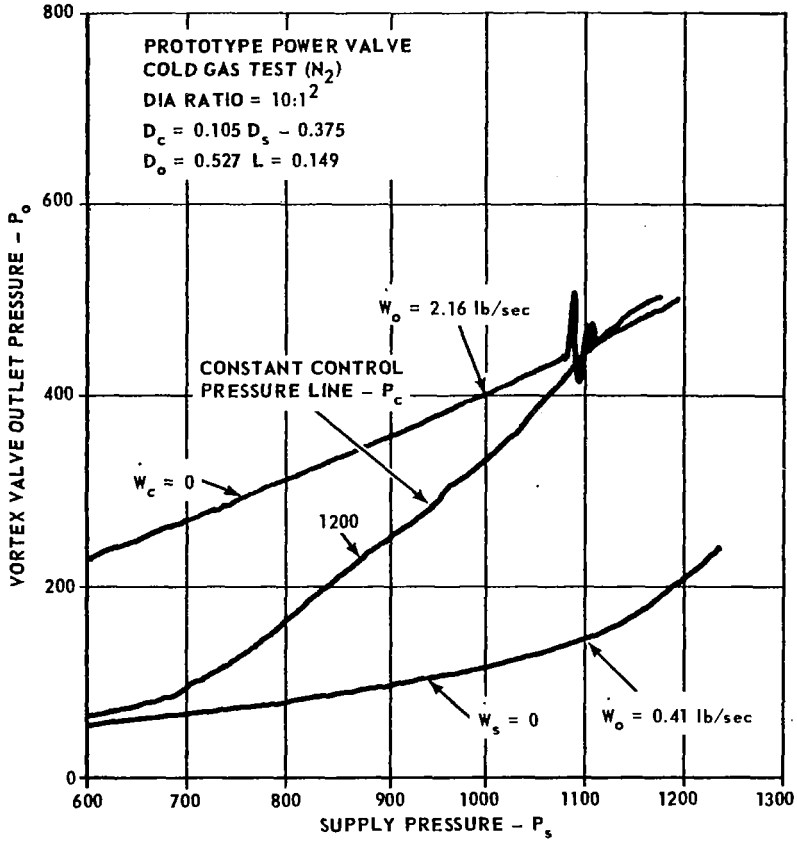

Figure 24 - Prototype Power Valve - Cold-Gas Test

totype model interfered with the control flow jet and degraded the control flow momentum. When the annulus area was doubled, the prototype valve characteristics resembled those of the breadboard model. Further evaluation during the breadboard valve test program would have indicated this significance of the annular clearance to injector diameter ratio.

System Hot-Gas Tests

Six hot-gas firings were made using the solid propellant gas generator. The first was for ballistic evaluation and acceptance of the gas generator. Five were complete system tests for evaluation of static and dynamic performance.

All system hot-gas tests were preceded by cold-gas tests to optimize system performance. The cold-gas tests were conducted using the high flow system shown schematically in Figure 25. This facility was designed for use of a high flow regulated source and tank blowdown which simulated the solid propellant gas generator flow characteristics. Pressure and flow distribution throughout the system was recorded on a direct-writing recorder. Data from the cold-gas tests was used to correlate hot-gas and cold-gas performance after a test firing.

Hot-Gas System Test No. 1 - The purpose of this test was to determine the system steady state performance, which includes total flow modulation and system pressure distribution. In addition, since this was the first firing, it provided necessary information about the insulation, seals, and control flow manifold. The basic system shown in Figure 26 was used for this test. No pilot valve was incorporated because dynamic response was not to be determined until a later test. Instead, a special manual poppet valve mounted on the power valve was used to modulate the control flow. This manual valve was actuated from a remote regulated nitrogen gas source.

This test lasted 8.1 seconds after ignition, at which time the power valve control line failed and system pressure dropped. Figure 27 shows the system before hot-gas test, and Figure 28 shows the hot-gas system performance. The hot-gas line which failed had too thin a wall to tolerate the high heat flux. Also, the supply manifold insulation eroded very badly. This was an asbestos-phenolic insert. Figure 29 shows the insulation before and after hot-gas Test No. 1. A high-density graphite liner was incorporated into the insulation inserts for the next test to provide structural integrity. The seals used throughout the system performed satisfactorily, and no other changes were required.

Hot-Gas System Test No. 2 - The second system firing was also performed to realize static performance data. The test installation included a new control flow manifold fabricated from a better high-temperature alloy. In addition, the system supply manifold insulation was improved by adding high-density graphite liners.

Except for some minor internal changes in the vortex regulator and power valve, the system configuration was the same as that used for Test No. 1. The power valve exit orifice area was increased to allow the system to operate at a slightly reduced supply pressure. This increased test time. It also minimized the possibility of over pressurization of the SPGG. Operating the system at a slightly lower system pressure does not affect the steady state performance. This was determined from cold-gas testing and normalizing the performance against system pressure ratios.

The duration of the hot-gas test was 38.8 seconds. This is approximately 8.0 seconds longer than the predicted burn time based on a supply pressure of 2300 psi. The SPGG supply pressure held nearly constant during the system test at 1875 psi and delivered 0.91 lb/sec. The system did not demonstrate full system flow modulation. This was primarily due to stroke limitation in the hot-gas manual valve. The system showed a modulation in output flow of 3.1 to 1.

The disassembled vortex valves after hot-gas Test No. 2 are shown in Figure 30. The supply flow manifold performed satisfactorily. The design of the manifolding and insulation was considered adequate for future tests.

Hot-Gas System Test No. 3 - The purpose for hot-gas Test No. 3 was to determine both system dynamic frequency response and static performance. The

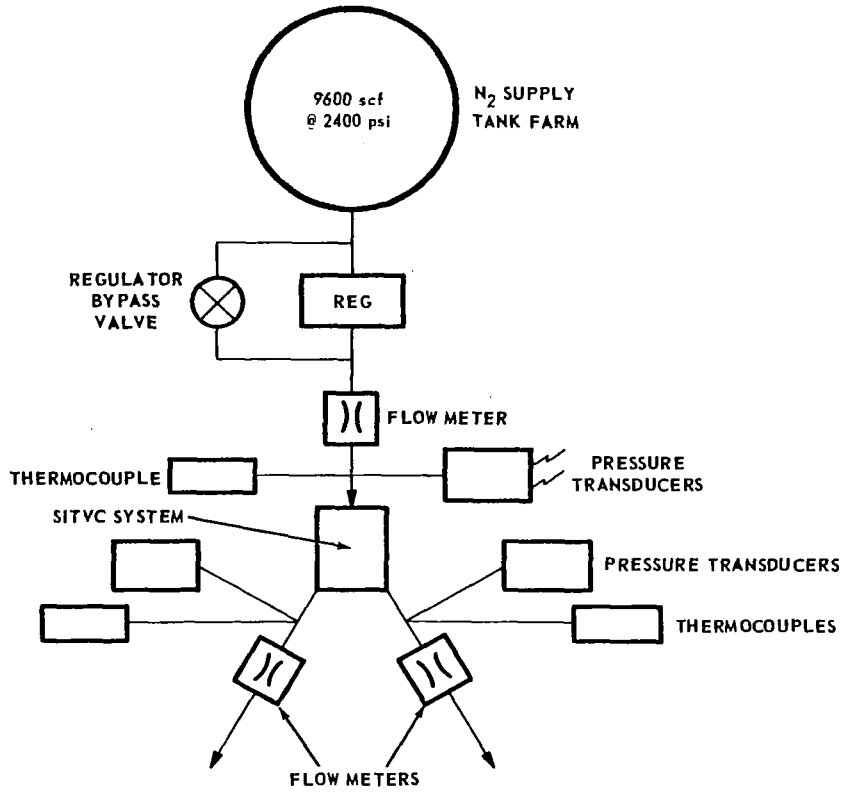

Figure 25 - Cold-Gas System Test Schematic

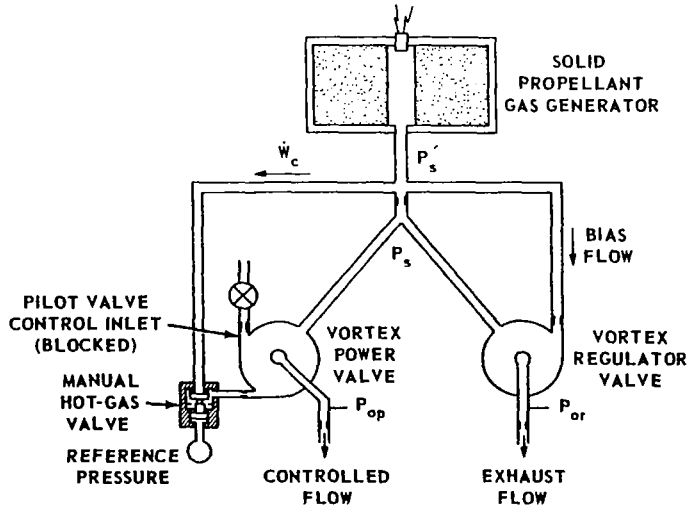

Figure 26 - Test Schematic - Hot-Gas Test No. 1

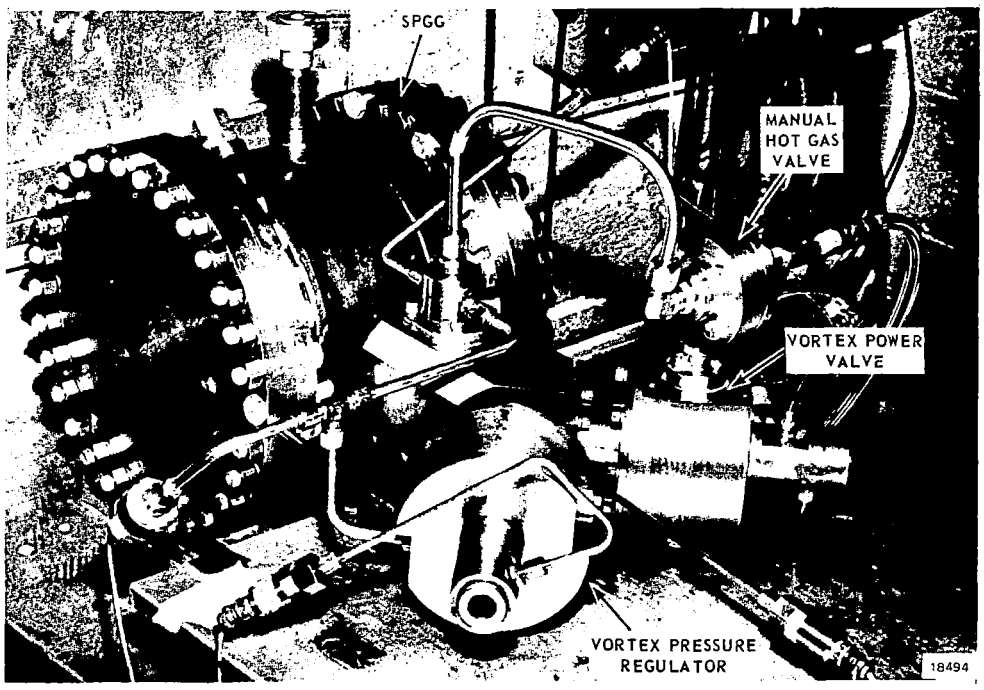

Figure 27 - System before Hot-Gas Test No. 1

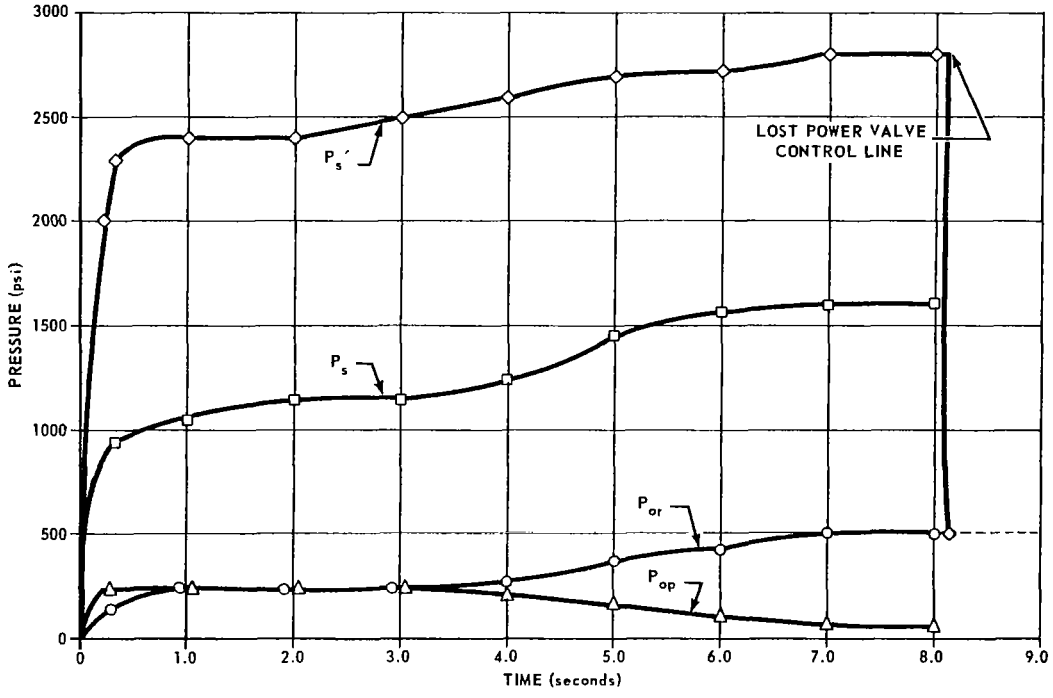

Figure 28 - Reduced Data - Hot-Gas Test No. 1

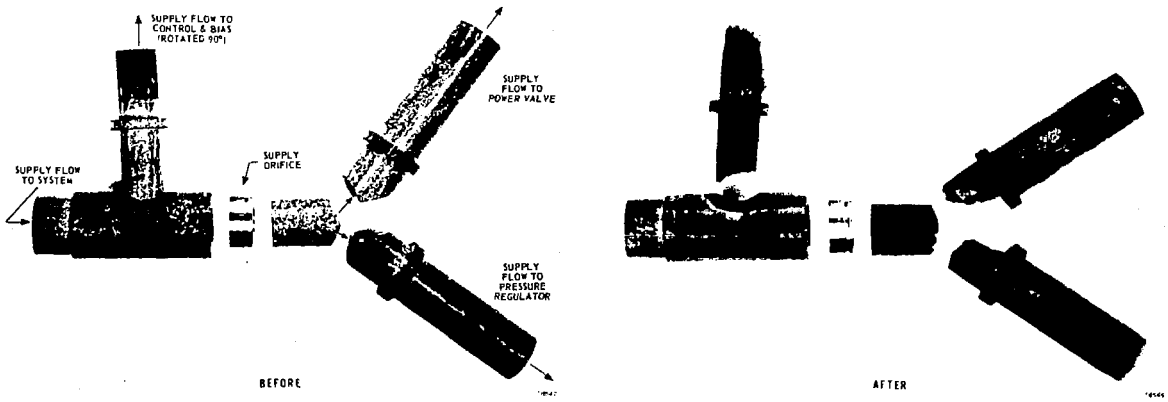

Figure 29 - Supply and Control Flow Insulators - Hot-Gas Test No. 1

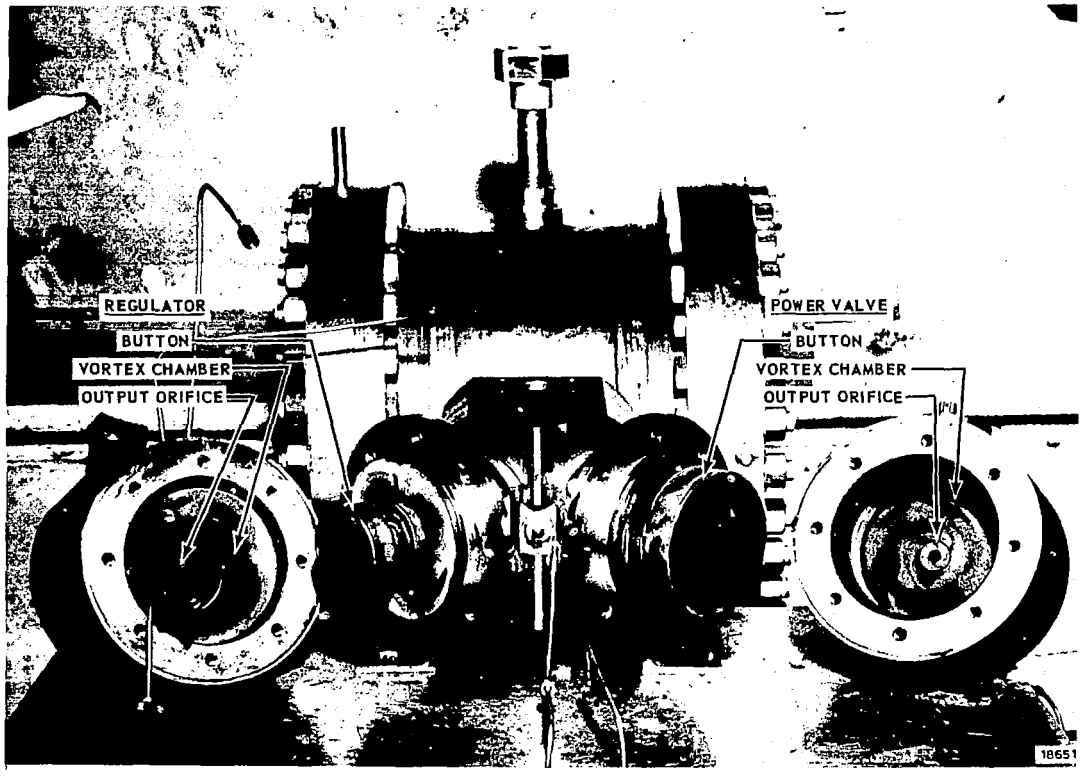

Figure 30 - Internal Parts after Hot-Gas Test No. 2

accomplishment of both tasks with a single hot-gas test required a change in the loading circuit for the manual hot-gas control valve.

A system schematic for this test is shown in Figure 31. The manual valve loading circuit No. 1 provided full control flow modulation by utilizing a preset pressure of 1400 psi. Loading circuit No. 2 provided a set pressure of 900 psi which positioned the manual valve to provide a system operating point near the center of the power valve flow modulation range. A bleed orifice was incorporated in the line supplying control pressure to the manual valve. Opening either of the solenoid valves resulted in a step input to the system. Closing the solenoid valve resulted in a modified ramp system input.

A bypass mechanical pressure regulator was added to the regulator valve bias flow line to maintain the bias pressure more nearly constant. The previous test showed that the wide variation in this pressure compromised the flow modulation performance severely. The flapper nozzle pilot valve was installed in parallel with the manual valve to introduce dynamic control inputs. A separate control flow injector was used for this valve.

The results of this test were good from a static performance standpoint. The firing lasted 31.3 seconds, 15.5 seconds of which were used to check static flow modulation performance. The remainder of the time was devoted to dynamic response testing. The total flow modulation measured at the power valve was 4.1 to 1. This was nearly identical with the cold-gas performance data. Vortex regulator and power valve output as a function of control to supply pressure ratio is plotted in Figure 32. The power valve output performance plotted against cold-gas performance data is shown in Figure 33. The gas generator burned at a supply pressure of 2200 psi and delivered a flow rate of 1.04 lb/sec based on 31.3 seconds burn time. The system pressure rise time was 0.20 second, which compares with previous generator ballistic tests.

No dynamic performance test data was obtained. Initially this was attributed to a clogged orifice in the pilot valve. It was later found to be a compound problem — a clogged supply orifice and a thermal relaxation of the pilot valve flapper-yoke assembly. After hot-gas Test No. 4 it was determined that the roll pins which fasten the flapper to the torque motor yoke assembly relaxed after a short exposure to the hot gas.

Hot-Gas System Test No. 4 - This test was conducted principally to realize system dynamic performance. An in-line dirt trap was added to the pilot valve supply line to prevent orifice clogging, which had been diagnosed as being responsible for failing to realize dynamic response data during hot-gas Test No. 3.

It was decided to bias the power valve to the center of the flow modulation range utilizing a fixed-area in-line orifice in place of the manual valve. This was included by removing the manual valve poppet and replacing the metering seat with the orifice. A schematic of the test system configuration is shown in Figure 34.

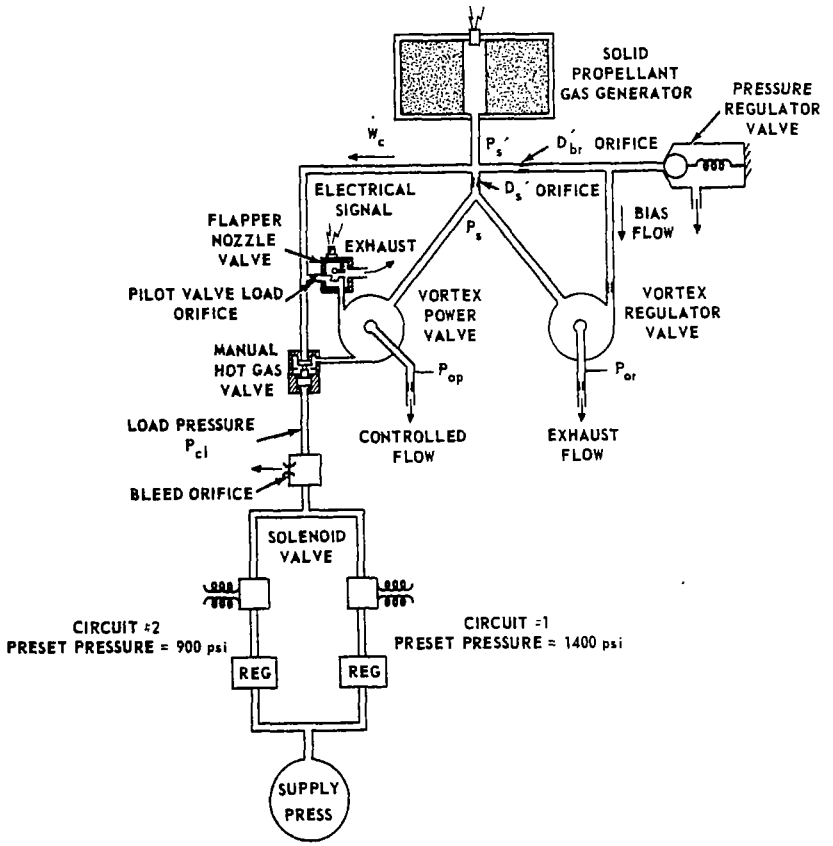

Figure 31 - Test Schematic - Hot-Gas Test No. 3

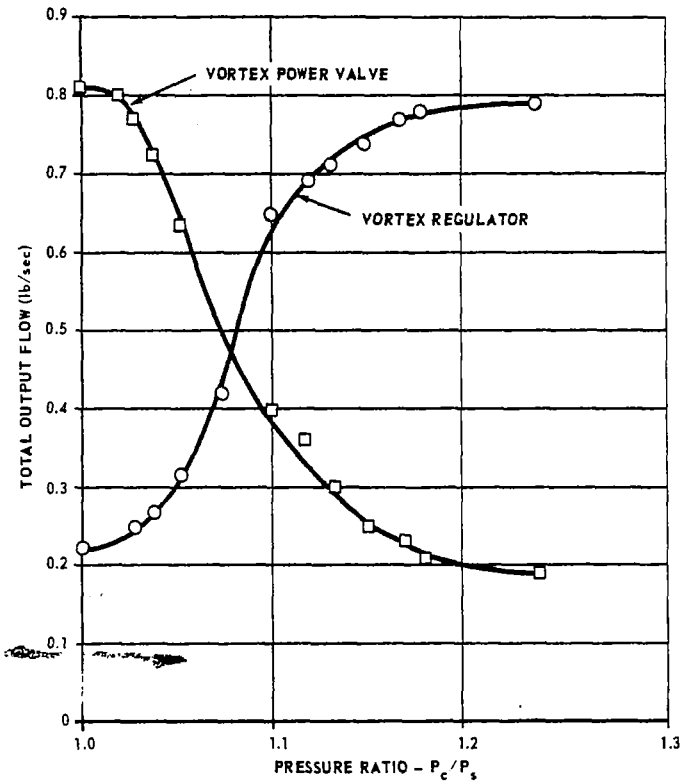

Figure 32 - Static Performance - Hot-Gas Test No. 3

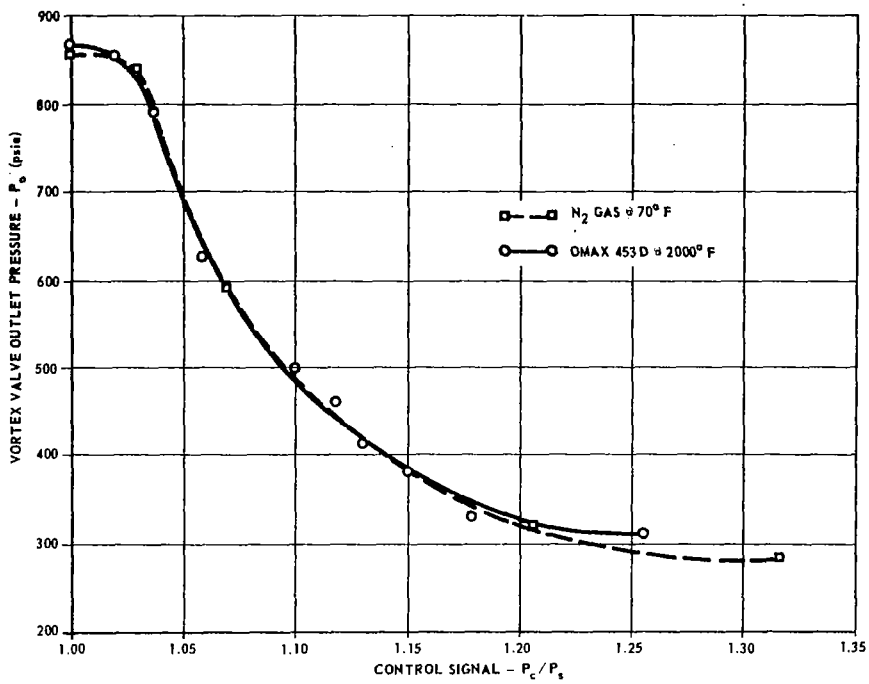

Figure 33 - Cold- and Hot-Gas Test Correlation - Hot-Gas Test No. 3

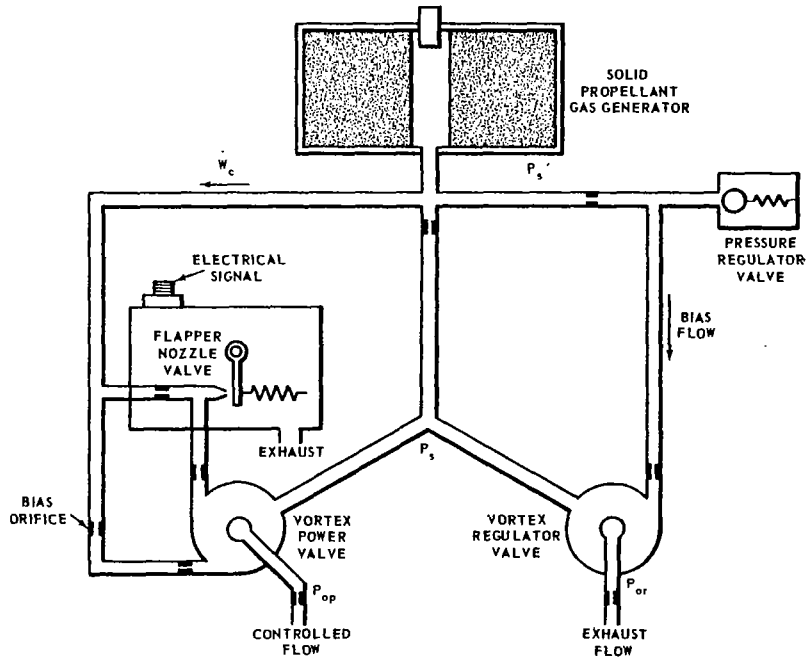

Figure 34 - Test Schematic - Hot-Gas Test No. 4 and No. 5

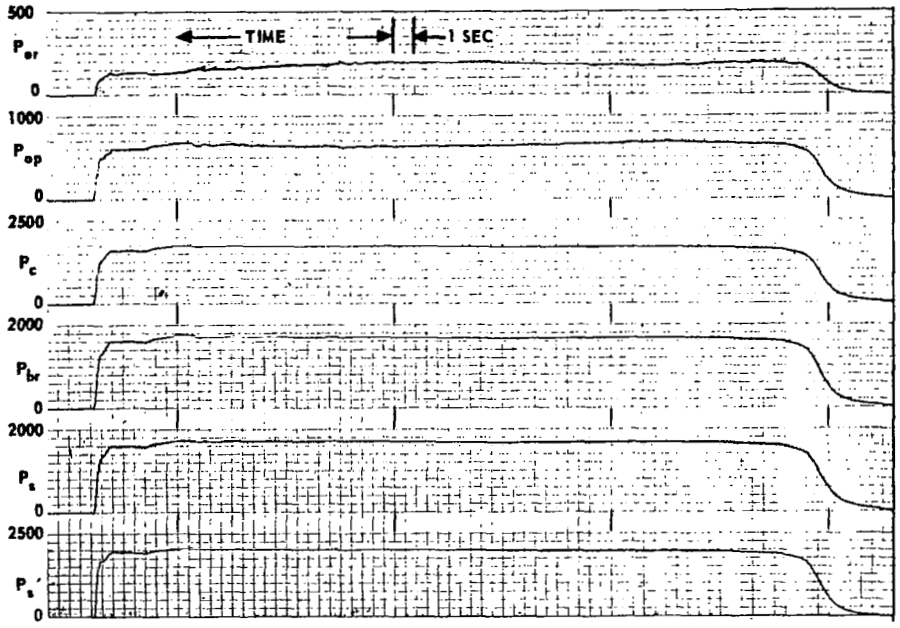

Figure 35 - Performance Data - Hot-Gas Test No. 4

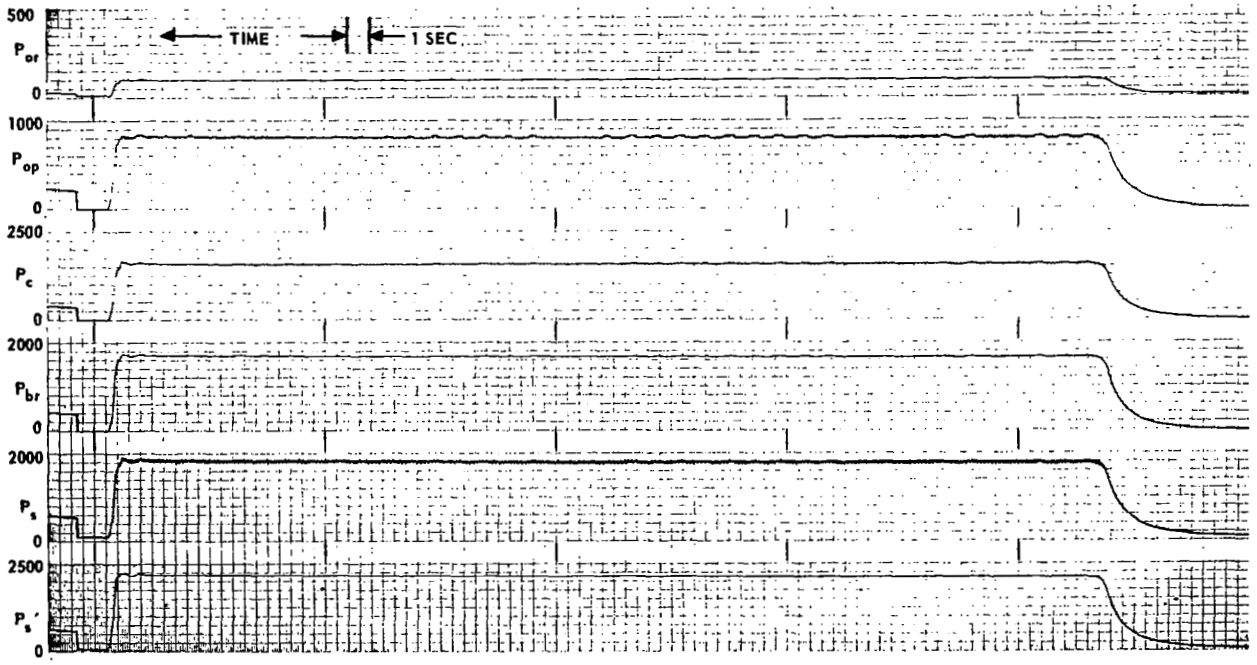

Figure 36 - Cold-Gas Test Data (System) prior to Test No. 4

This hot-gas test lasted 32.5 seconds. The average generator supply pressure was 1990 psi and the flow rate was 1.02 lb/sec. The objective of realizing frequency response data was not achieved. The control flow input was only sinusoidally varied for the first few seconds. It was deduced that the pilot valve flapper was being deflected relative to the torque motor drive yoke. This resulted from relaxation of the roll pins used to fasten the flapper to the yoke. A sequence of pilot valve firings, using a smaller solid propellant gas generator, was undertaken after this firing to correct the problem.

The primary accomplishment of Test No. 4 was in proving the stability of the vortex valves during the full duration of a hot-gas test. The supply pressure only changed about 2 1/2 percent from normal expected variation, a surprisingly low value. Figure 35 shows the results for the hot-gas test, and Figure 36 shows the results of a prior cold-gas test.

Hot-Gas System Test No. 5 - The purpose of hot-gas Test No. 5 was to evaluate system frequency response to 30 cps and response to a step input signal. This was to be compared with cold-gas performance for dynamic correlation. The system configuration used for this test is identical to that of Test No. 4 shown in Figure 34. The problem with the pilot stage flapper mounting pins relaxing was eliminated by fabricating the flapper and torque motor drive yoke as a single unit. The pilot valve was hot-gas tested prior to this system firing.

The test duration was 34 seconds, of which 27 seconds were used for sinusoidal response of the system. The balance of the test run was used for step input response evaluation. The system dynamic sinusoidal frequency response up to 30 cps was plotted from the test data (Figure 37). System performance on cold gas is shown in Figure 38. Hot-gas system performance is shown in Figure 39. The sinusoidal frequency response at various frequencies is shown in Figures 40 through 43. The wave shape is distorted by the noise, inherent in the exiting vortex chamber flow. This noise appears on all of the vortex devices tested to

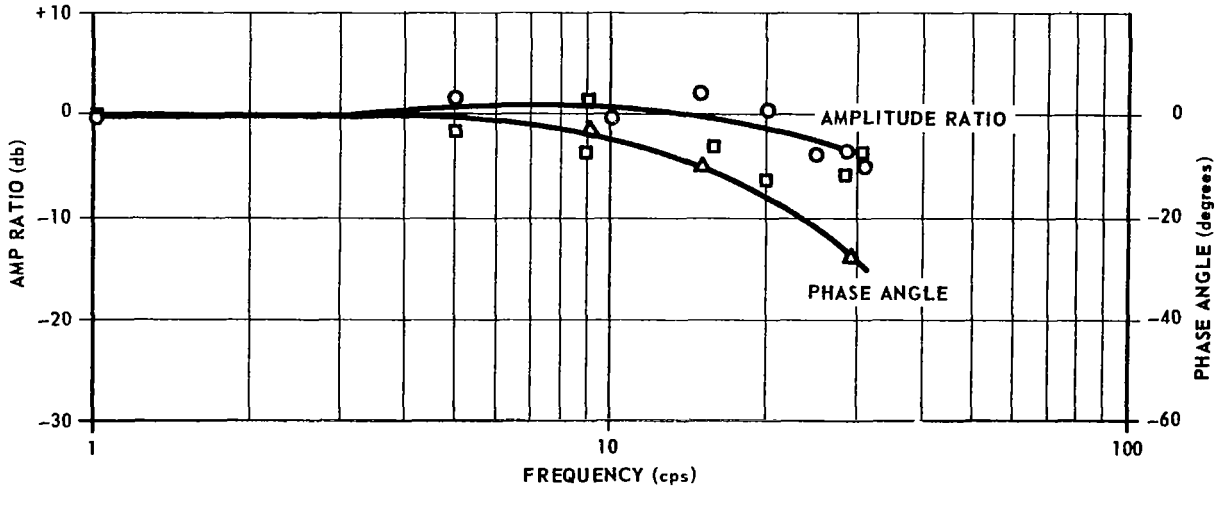

Figure 37 - System Frequency Response - Hot-Gas Test No. 5

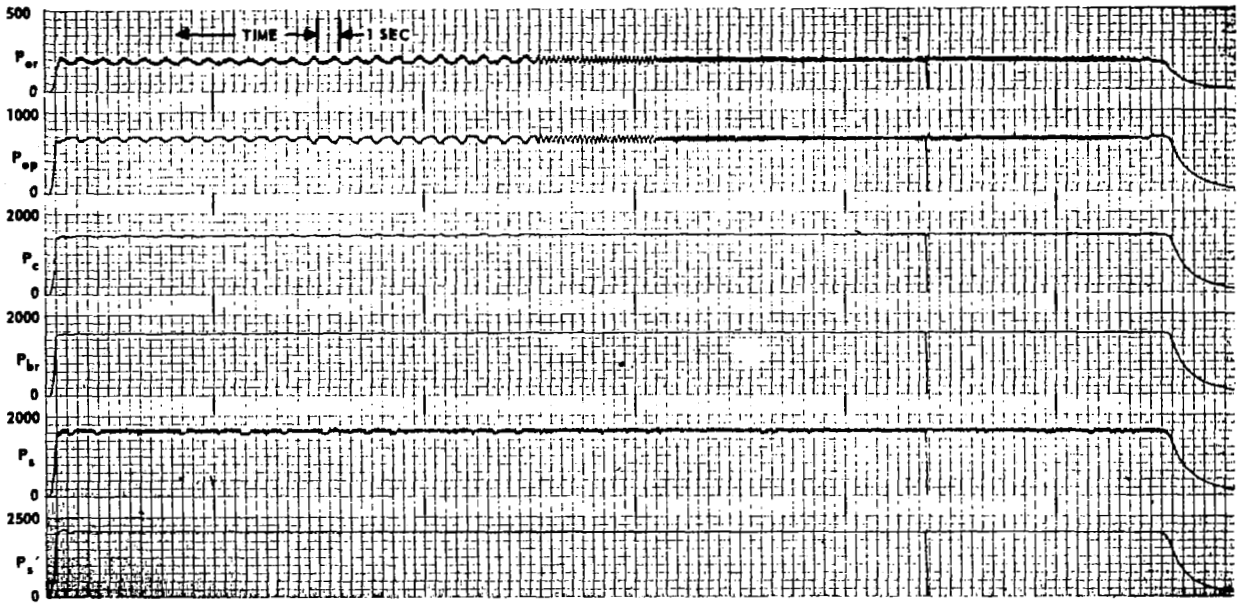

Figure 38 - Cold-Gas Test Data (System) prior to Test No. 5

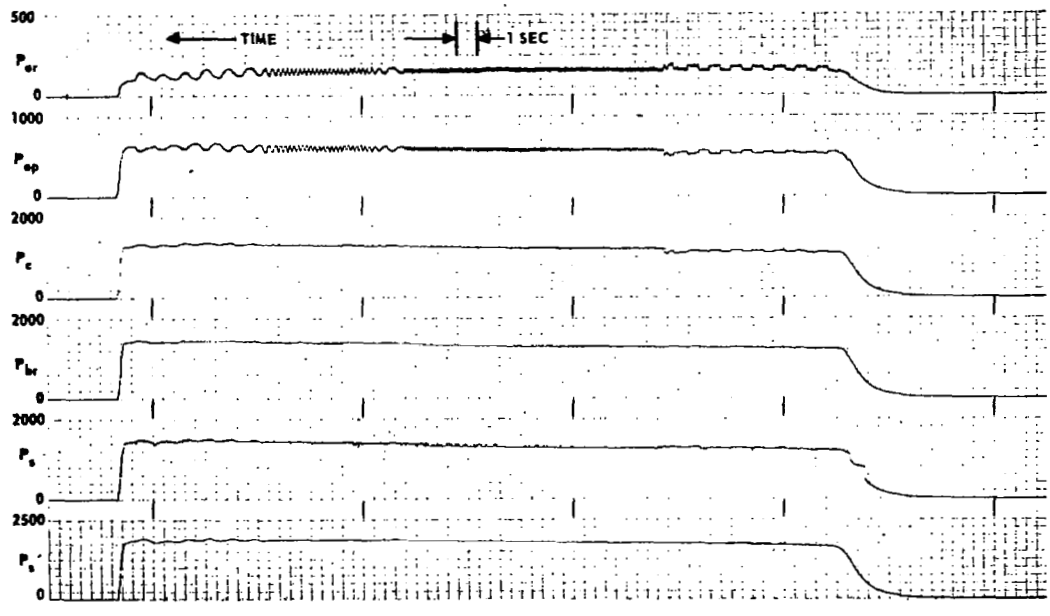

Figure 39 - Hot-Gas System Test

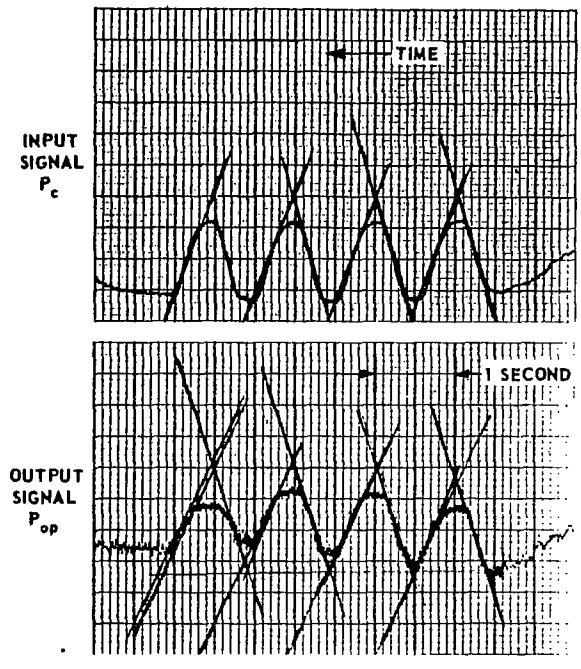

Figure 40 - Hot-Gas Frequency Response (1 cps)

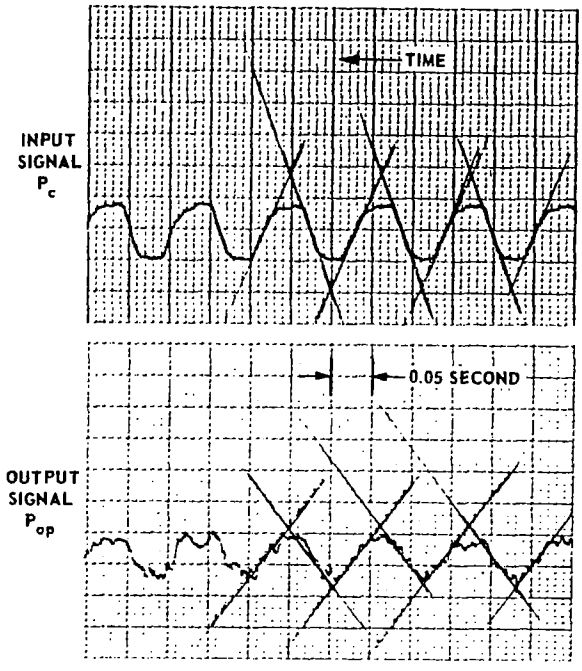

Figure 41 - Hot-Gas Frequency Response (10 cps)

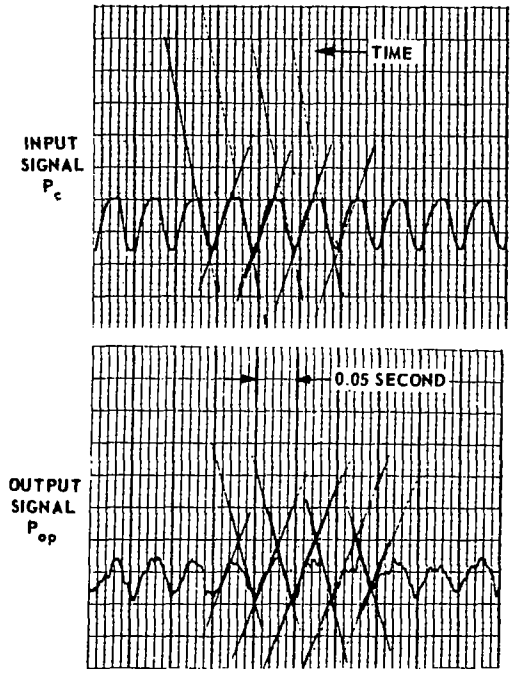

Figure 42 - Hot-Gas Frequency Response (20 cps)

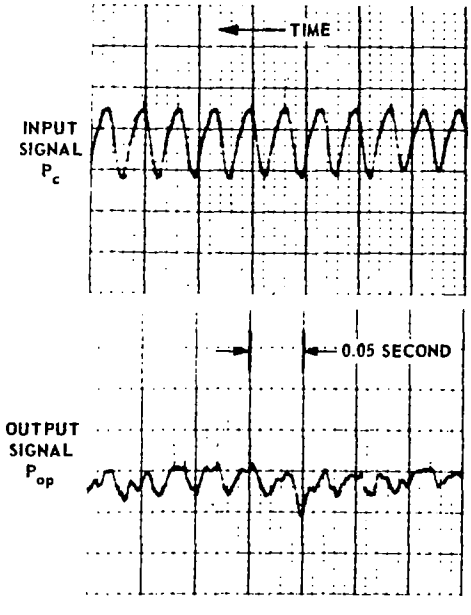

Figure 43 - Hot-Gas Frequency Response (30 cps)

date. In fact, it is one of the principal development areas for improving performance of high gain vortex devices where signal to noise ratio is significant. The exiting vortex valve flow is stagnated in a plenum volume which includes an exit load area for flow measurement. The plenum could be made large to allow stagnation of the flow, and the pressure transducer for measuring plenum chamber pressure could be installed in a relatively noisefree location. This, however, compromises the dynamic response measurement since the volume is the significiant time lag in the system . A method of measurement must be developed for this type of measurement.

The system showed an amplitude attenuation of -4db at 30 cps and a phase lag of 28 degrees. The response for this test was severely compromised by the large manifold volumes throughout the system. A lightweight system design would achieve considerably better response by eliminating volumes through close-coupling system components. Transient response is shown in Figure 44.

Evaluation of Test Results - The purpose, test system description, and results of the five hot-gas tests conducted during this program are summarized in Table 7. The test system demonstrated a hot-gas flow modulation range of 4.1 to 1, shown in Figure 32. The hot-gas test correlation with cold-gas test was exceptionally good as shown in Figure 33 on a normalized plot of output flow ratio versus control to supply pressure ratio. Test No. 4, an effective steady state test of the system, demonstrated the insensitivity to thermal transients. System pressures were maintained constant within 2 1/2 percent without a shift in operating point.

System frequency response was demonstrated in Test No.5. The system was dynamically tested with a sinusoidal control signal input up to 30 cps. At 30 cps the amplitude ratio attenuation was -4 db with a phase lag of 28 degrees. The demonstrated response is sufficient for most thrust vector control requirements but is capable of improvement by minimizing manifold volumes in flight hardware. The system demonstrated was intended primarily for feasibility determination, and optimization of hardware for best dynamic response was not accomplished.

The system chosen, incorporating the vortex power valve and vortex regulator with active control only on the power valve, proved to be a difficult system for optimizing the flow modulation range. Matching the characteristics of the high gain regulator valve required considerable cold-gas testing, and finally a problem was encountered in maintaining the regulator valve bias control pressure constant. A better system operating mode would be to operate both valves as power valves with active control supplied to each in a push-pull manner. This system would be symmetrical, and the use of staging between the pilot valve and final power valves would exhibit wide range flow modulation and high total flow gain.

The system test hardware performed reasonably well with the exception of the problem with the manifold insulation which was corrected after system firing No. 1. The insensitivity of the vortex valve to thermal transients was apparent from the consistent system performance throughout each hot-gas test.

Table 7 - Summary of Hot-Gas System Tests

Test	Purpose	Description	Results	Duration (seconds)
1	Steady state performance evaluation	Basic system; No pilot valve; Hot-gas manual valve used for modulation	Control line ruptured; Manifold insulation failed	8.2
2	Steady state performance evaluation	Basic system; No pilot valve; Hot-gas manual valve used for modulation	Operated system at lower supply pressure; Flow modulation 3.1 to 1; Manual valve stroke limited	38.8
3	Steady state and Dynamic performance	Basic system; Pilot valve; Manual valve; Pressure regulator valve installed in vortex regulator bias control line	Flow modulation 4.1 to 1; No frequency response data; Pilot valve failure	31.3
4	Dynamic performance	Basic system; Pilot valve; Vortex power valve biased to operating point; No manual valve; Pressure regulator installed	Pilot valve failed; Test indicated thermal stability of system	32.0
5	Dynamic performance	Same as Test No. 4	30 cps frequency response data; Step response data	34.0

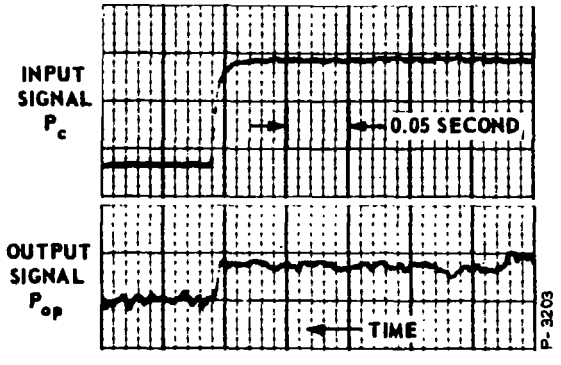

Figure 44 - Hot-Gas Transient Response

CONCLUSIONS AND RECOMMENDATIONS

Conclusions

The fluid state vortex valve secondary injection control system shows considerable promise for future application to solid propellant rocket engine thrust vector control. Based on the program described in this report, the following conclusions are apparent:

1. The system demonstrated showed a total flow modulation range of 4.1 to 1 for both cold-gas and hot-gas tests.

2. Frequency response to a sinusoidal control input showed an amplitude ratio attenuation of -4 db at 30 cps with a concurrent phase lag of 28 degrees. This was a feasibility system without optimized design, and the major limitations in response were the associated manifold volumes. These could be reduced in a flight-weight system for improved dynamic performance.

3. The system was tested using cold nitrogen gas and hot gas supplied from a solid propellant gas generator. The performance with regard to total flow modulation range and gain was nearly identical in both cases. Performance normalizes very well, and extrapolation of performance to applications with different gas sources can be achieved with good accuracy.

4. The system chosen for demonstration included a vortex power valve and a vortex regulator valve. The power valve had active control supplied by an electropneumatic pilot valve. The regulator valve operated by introducing a bias flow set by a fixed orifice. This is basically an unsymmetrical system and required considerable matching of characteristics to achieve acceptable performance. The maximum flow modulation capability of the individual vortex valves was never achieved from the system tests because of the problem with matching performance. A better choice of system would be to operate both valves with active control in push-pull. In addition, staging, or the addition of two more vortex valves between the pilot valve and the power valves, would improve total flow gain.

5. The vortex valve scales very accurately. Considerable cold-gas testing was accomplished using scale models. The parameter variation studies resulted in basic insight into the effect of design parameters on performance. This basic understanding can be applied effectively to all future design of vortex valves for any type of application.

Recommendations

The feasibility of the vortex valve for application to a secondary injection control system operating with gases produced from a solid propellant gas generator has been demonstrated. A basic understanding of the problems attendant to this type of application with regard to thermal transients, gas contamination, and choice of system schematic has been achieved.

The next logical step is to apply the knowledge gained to the development of a complete system designed to operate with higher temperature gas. The ultimate goal is to bleed the rocket engine combustion chamber. This means that the system must be capable of handling gases with temperatures up to 6500°F. The solid propellants supplying these gases have a high aluminum content. The increase from a 2000°F, relatively clean propellant to 6500°F is considered to be too extreme. It is recommended that a propellant composition providing gas somewhere in the order of 5500°F with an aluminum content in the order of 16 percent be chosen. The development of this high-temperature system hinges on selection of materials and proper design installation of these materials. The vortex valve flow passages must be built from materials which can tolerate the erosive gas, as well as being capable of achieving a high surface temperature quickly to prevent excessive deposition of aluminum oxide which is carried in the gas.

A new system schematic should be utilized in place of the assymmetric system demonstrated. A push-pull system including staging, as shown in Figure 45, would be more ideal. This is completely symmetrical and includes active control of both power stage valves.

A complete heat transfer and stress analysis of the vortex valve operating with the aluminized high-temperature gas is mandatory. This would dictate the type and design of the insulation materials required. It would also be used in combination with the known fluid mechanics relationships of the vortex valve to predict flow field velocities. This would give insight into potential problems resulting from localized erosion caused by change in direction of the hot gas and resultant local concentration of the aluminum oxide.

The next phase of development should include designing hardware as light weight as possible to provide accurate weight and life estimates for tradeoff with other types of systems. The final criteria for selection of a system are based on consideration of weight, life, response, configuration, reliability, and cost.

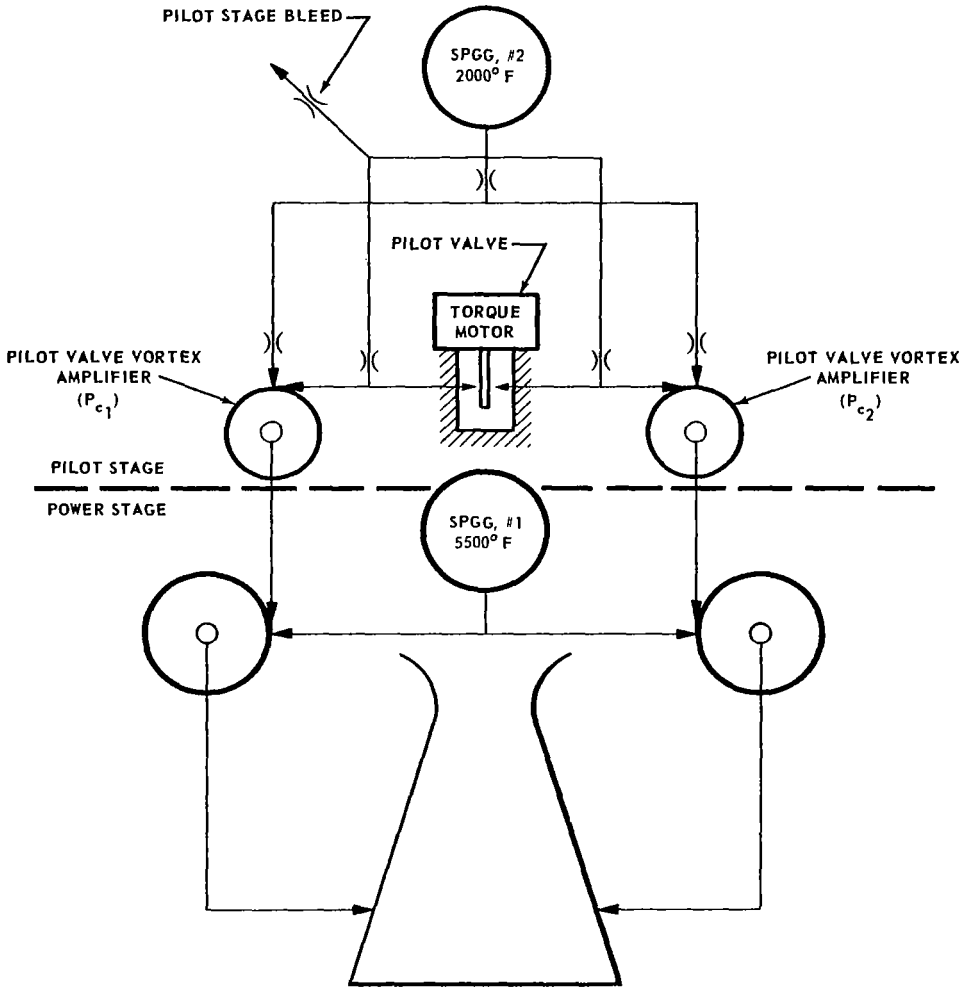

Figure 45 - Push-Pull, Symmetrical 5500°F SITVC System

APPENDIX A

STEADY STATE ANALYSIS FOR THE 2000°F SITVC SYSTEM

Summary

This analysis provides a basic mathematical system model from which steady state system performance can be evaluated. It also provides a correlation factor for the difference when operating with ammonium nitrate solid propellant gas or nitrogen gas. System design parameters for both hot and cold gas are summarized in Table A-1. The analysis is based on the following assumptions:

(1) Thermodynamic properties of Olin-Mathieson OMAX 453D solid propellant

Table A-1 - System Design Parameter Summary

	Hot Gas	Cold Gas
P_s'	2265	2265
P_s(max.)	1865	1865
P_s(min.)	1730	1730
P_c	2215	2215
P_{op}	900	900
P_{br}	1865	1865
P_{or}	As Required	As Required
$\dot{W}_s'$	1.04	2.86
$\dot{W}_c$	0.176 (max.)	0.504
$\dot{W}_{op}$(max.)	0.88	2.51
$\dot{W}_{op}$(min.)	0.176	0.504
$\dot{W}_{br}$	0.16 (max.)	0.457
$\dot{W}_{or}$(max.)	0.792	2.26
$\dot{W}_{or}$(min.)	0.16	0.457

NOTE: All pressures in psig
All flows in lb/sec

(2) Constant generator pressure

(3) Negligible thermal losses throughout the system

(4) No change in area of control orifices

(5) Gases obey ideal gas laws

Basic Flow Equations

The basic equation for flow through an orifice (see Reference 2) is:

$$\dot{W} = C\, C_d\, A\, \frac{P_u}{\sqrt{T_u}}\, f_1\left(\frac{P_d}{P_u}\right) \tag{1}$$

$f_1\left(\frac{P_d}{P_u}\right)$ is calculated from:

$$f_1\left(\frac{P_d}{P_u}\right) = \frac{\left(\frac{P_d}{P_u}\right)^{\frac{1}{k}} \sqrt{1 - \left(\frac{P_d}{P_u}\right)^{\frac{k-1}{k}}}}{\left[\left(\frac{P_d}{P_u}\right)^{\frac{1}{k}} \sqrt{1 - \left(\frac{P_d}{P_u}\right)^{\frac{k-1}{k}}}\right]_{\max.}} \tag{2}$$

If $\left(\frac{P_d}{P_u}\right)$ is less than $\left(\frac{P_d}{P_u}\right)_{\text{critical}}$

then:

$$f_1\left(\frac{P_d}{P_u}\right) = 1 \quad \text{(for sonic flow conditions)}$$

and

$$\left(\frac{P_d}{P_u}\right)_{\text{critical}}$$

is given by:

$$\left(\frac{P_d}{P_u}\right)_{\text{critical}} = \left(\frac{2}{k+1}\right)^{\frac{k}{k-1}}$$

and

$$C = \frac{\sqrt{\frac{kg}{R}}}{\left(\frac{k+1}{2}\right)^{\frac{k+1}{2(k-1)}}} \qquad (3)$$

The thermodynamic properties of OMAX 453D are:

$k = 1.30$

$\overline{m} = 18.4$ lb/mole

$T = 2460°R$

$R = 1009 \frac{\text{in.-lb}}{\text{lb-°R}}$

Then:

$$\left.\frac{P_d}{P_u}\right|_{\text{critical}} = 0.547$$

and

$$C = 0.412 \quad \frac{°R^{1/2}}{\text{sec}}$$

The thermodynamic properties of Nitrogen are:

$k = 1.4$

$\overline{m} = 28$ lb/mole

$T = 530°R$

$R = 662 \frac{\text{in.-lb}}{\text{lb-°R}}$

Then:

$$\left.\frac{P_d}{P_u}\right|_{\text{critical}} = 0.528$$

and

$$C = 0.523 \quad \frac{{}^{\circ}R^{1/2}}{sec}$$

Hot-Gas and Cold-Gas Correlation

Since the cold-gas test medium will be gaseous nitrogen, it is necessary to establish equivalent parameters based on the thermodynamic properties of the two gases. The selected common parameter is pressure; therefore a derivation for equivalent flow is required.

Starting with the basic equation for subsonic flow and equating those terms which depend on thermodynamic properties to the independent terms and the common parameter, pressure, yields:

$$\frac{\dot{W}\sqrt{T_u}}{C f_1\left(\frac{P_d}{P_u}\right)} = C_d A P_u = \text{Constant} \tag{4}$$

C_d and A are functions of the control area geometry. P is the common parameter between the hot and cold gas. Equating the dependent terms,

$$\left.\frac{\dot{W}\sqrt{T_u}}{C f_1\left(\frac{P_d}{P_u}\right)}\right|_{OMAX} = \left.\frac{\dot{W}\sqrt{T_u}}{C f_1\left(\frac{P_d}{P_u}\right)}\right|_{N_2} \tag{5}$$

Solving for the equivalent weight flow of hot gas in terms of cold gas yields:

$$\dot{W}_{OMAX} = \dot{W}_{N_2}\left(\frac{C_{OMAX}}{C_{N_2}}\right)\left(\frac{T_u N_2}{T_u OMAX}\right)^{\frac{1}{2}} \frac{f_1\left(\frac{P_d}{P_u}\right)_{OMAX}}{f_1\left(\frac{P_d}{P_u}\right)_{N_2}} \tag{6}$$

Assuming both flows sonic:

$$\dot{W}_{OMAX} = 0.365\ \dot{W}_{N_2}$$

If either flow is subsonic:

$$\dot{W}_{OMAX} = 0.365\ \dot{W}_{N_2} \left[\frac{f_1 \left(\frac{P_d}{P_u}\right)_{OMAX}}{f_1 \left(\frac{P_d}{P_u}\right)_{N_2}} \right]$$

Minimum Vortex Valve Supply Flow Approach Area

The pressure drop in the supply flow line to the vortex valve is minimized by holding the Mach number below 0.15. For design purposes a relationship between line pressure, flow, and area is used. The following is the derivation:

$$C^* = \sqrt{g\,k\,R\,T} \tag{7}$$

$$\dot{W} = \tilde{V} A\, P_u / R\,T \tag{8}$$

$$M = \frac{\tilde{V}}{C^*} \tag{9}$$

$$R = \overline{R}/\overline{m} \tag{10}$$

$$A = \frac{\dot{W}}{M P_u} \sqrt{\frac{R\,T}{k\,g}} \tag{11}$$

Evaluating the constants in terms of approach area, flow, and pressure for a Mach number of 0.15 yields:

$$A = 417\ \frac{\dot{W}}{P_u}\ \text{in.}^2\ \text{(min.)} \tag{12}$$

Steady State System Analysis Vortex Valve Design Requirements

The following are design requirements for the vortex valves. The optimized design parameters were established by cold-gas testing of scale models of the vortex regulator and power valve. The vortex power valve design requirements are:

$$\left.\frac{P_c}{P_s}\right|_{\text{max.}} = 1.28$$

$$\left.\frac{P_{op}}{P_s}\right|_{max.} = 0.52$$

$$\left.\frac{\dot{W}_c}{\dot{W}_{op}}\right|_{max.} = 0.196$$

The vortex regulator valve design requirements are:

$$\left.\frac{P_{br}}{P_s}\right|_{max.} = 1.08$$

$$\left.\frac{P_{or}}{P_s}\right|_{max.} = 0.49 \text{ max.}$$

$$\left.\frac{\dot{W}_{br}}{\dot{W}_{or}}\right|_{max.} = 0.18$$

System Flow Distribution

A flow summation equation is written at each pressure level to determine the system flow distribution. Starting at the SPGG, each requirement of the system circuit (Figure A-1) is removed and the summation equation is written. The summation of flow upstream of the A_s' orifice is shown in Figure A-2.

$$\dot{W}_s' = \dot{W}_{br}' + \dot{W}_c + \dot{W}_s \tag{13}$$

The summation of flow between A_s', A_{sp}', and A_{sr} is shown in Figure A-3.

$$\dot{W}_s = \dot{W}_{or} - \dot{W}_{br} + \dot{W}_{op} - \dot{W}_c \tag{14}$$

The flow through the A_{op} and A_{or} orifices is shown in Figure A-4.
The summation of flow between A_{br}' and A_{br} is shown in Figure A-5.

$$\dot{W}_{br}' = \dot{W}_{br} + \dot{W}_{bl} \tag{15}$$

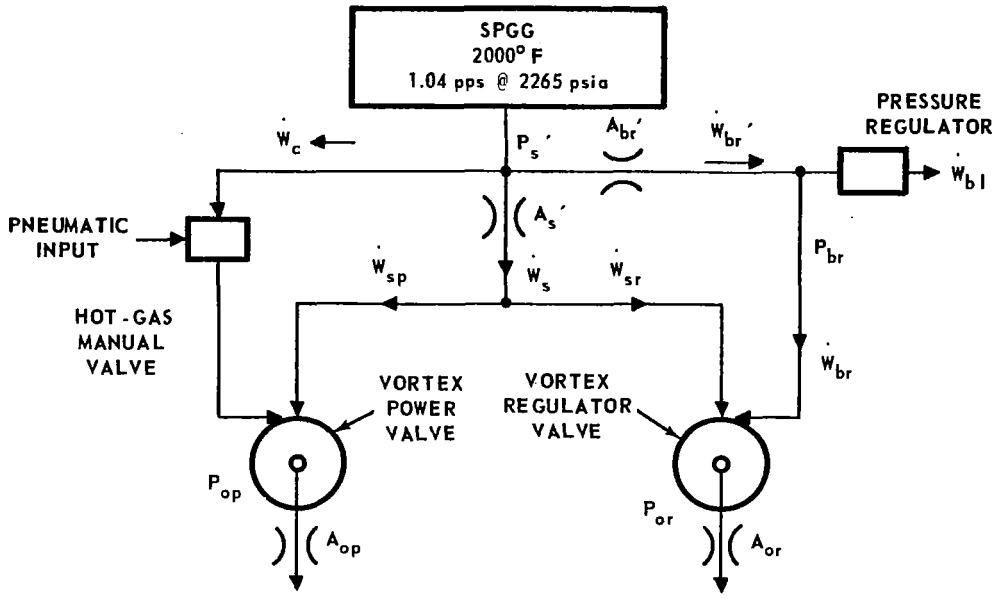

Figure A-1 - System Flow Model

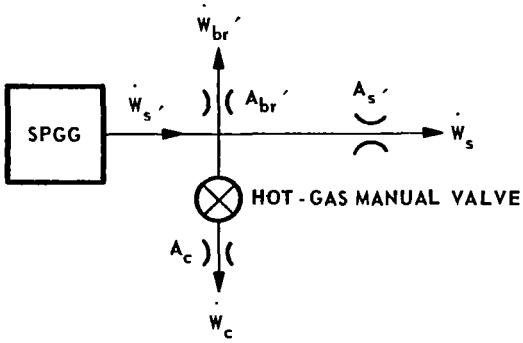

Figure A-2 - Subsystem Schematic 1

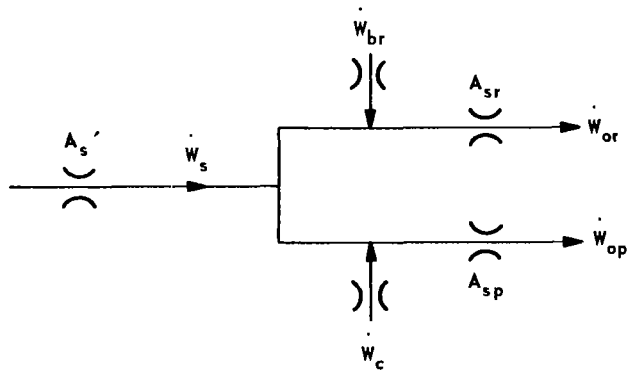

Figure A-3 - Subsystem Schematic 2

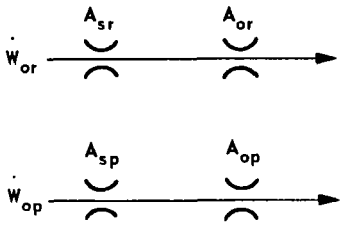

Figure A-4 - Subsystem Schematic 3

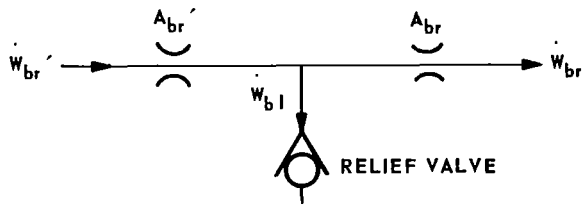

Figure A-5 - Subsystem Schematic 4

Power Valve Flowing Maximum

Assume power valve is flowing maximum (the hot-gas manual valve is closed). Substituting equation (14) into equation (13) and solving for $\dot{W}_s$ yields:

$$\dot{W}_s = \dot{W}_{br}' - \dot{W}_{br} + \dot{W}_{or} + \dot{W}_{op} \tag{16}$$

Since $\dot{W}_{br}' - \dot{W}_{br}$ is equal to the relief valve exhaust flow and is negligible during this mode:

$$\dot{W}_s = \dot{W}_{or}\,(\text{min.}) + \dot{W}_{op}\,(\text{max.}) \tag{17}$$

Power Valve Flowing Minimum

Assume the power valve is completely turned down (the hot-gas manual valve is open). Substituting equation (14) into equation (13) for $\dot{W}_s$ and $\dot{W}_{br}' - \dot{W}_{br}$ yields:

$$\dot{W}_s' = \dot{W}_{bl} + \dot{W}_{or}\,(\text{max.}) + \dot{W}_{op}\,(\text{min.}) \tag{18}$$

It was determined during cold-gas tests that the regulator could be modulated through a 5:1 turndown range using 45 percent of the required total control bias flow. Expressing the required exhaust flow in terms of bias flow:

$$\dot{W}_{bl}\,(\text{max.}) = 0.45\,\dot{W}_{br}\,(\text{max.}) \tag{19}$$

and

$$\dot{W}_{br}\,(\text{max.}) = \frac{\dot{W}_{or}}{5}\,(\text{max.}) \tag{20}$$

To realize a 5:1 total flow modulation from the power valve, the minimum output flow must be:

$$\dot{W}_{op}\,(\text{min.}) = \frac{1}{5}\,\dot{W}_{op}\,(\text{max.}) \tag{21}$$

Substituting equations (19), (20), and (21) into equations (17) and (18) yields:

$$\dot{W}_s' = \frac{\dot{W}_{or}}{5}\,(\text{max.}) + \dot{W}_{op}\,(\text{max.}) \tag{22}$$

$$\dot{W}_s' = \frac{0.45}{5}\,\dot{W}_{or}\,(\text{max.}) + \dot{W}_{or}\,(\text{max.}) + \frac{\dot{W}_{op}}{5}\,(\text{max.}) \tag{23}$$

$$\dot{W}_s' = 1.09\ \dot{W}_{or}\ (\text{max.}) + \frac{\dot{W}_{op}}{5}\ (\text{max.})$$

Multiplying equation (22) by 1.09 and dividing equation (23) by 5 yields:

$$1.09\ \dot{W}_s' = \frac{1.09}{5}\ \dot{W}_{or}\ (\text{max.}) + 1.09\ \dot{W}_{op}\ (\text{max.}) \tag{24}$$

$$\frac{\dot{W}_s'}{5} = \frac{1.09}{5}\ \dot{W}_{or}\ (\text{max.}) + \frac{\dot{W}_{op}}{25}\ (\text{max.}) \tag{25}$$

Subtracting equation (24) from equation (25):

$$\dot{W}_s'\ (1.09 - 0.2) = \dot{W}_{op}\ (\text{max.})\ (1.09 - 0.04) \tag{26}$$

$$\dot{W}_{op}\ (\text{max.}) = \frac{0.89}{1.05}\ \dot{W}_s' = 0.88\ \text{lb/sec}$$

$$\dot{W}_{op}\ (\text{min.}) = 0.176\ \text{lb/sec}$$

$$\dot{W}_{or}\ (\text{min.}) = 0.16\ \text{lb/sec}$$

From equation (11):

$$\dot{W}_{or}\ (\text{max.}) = \frac{1.04 - 0.176}{1.09} = \frac{0.864}{1.09} = 0.792\ \text{lb/sec}$$

and

$$\dot{W}_{bl}\ (\text{max.}) = 0.072\ \text{lb/sec}$$

Since at minimum valve turndown the output is equal to the control flow:

$$\dot{W}_{br}\ (\text{max.}) = 0.16\ \text{lb/sec}$$

$$\dot{W}_c\ (\text{max.}) = 0.176\ \text{lb/sec}$$

System Pressure Distribution

To determine the required pressure distribution which will satisfy the flow output from the vortex power valve, the pressure upstream of the power valve plenum chamber is set as follows:

$$P_{op}\ (\text{max.}) = 900\ \text{psia}$$

$$P_s\ (\text{min.}) = 1730\ \text{psia}$$

The actual supply pressure change will be determined after the vortex valves are sized.

Power Valve Design

Based on knowledge of the required input and output pressures and flows, the vortex power valve can be sized using the basic flow equation (1):

$$A_{op} = \frac{\dot{W}_{op}\sqrt{T}}{C_d C P_{op}} = \frac{0.88\sqrt{2460}}{0.87 \times 0.412 \times 900} = 0.136 \text{ in.}^2$$

$$A_{sp} = \frac{\dot{W}_{op}\sqrt{T}}{C_d C P_s} = \frac{0.88\sqrt{2460}}{0.87 \times 0.412 \times 1730} = 0.0707 \text{ in.}^2$$

$$A_c = \frac{\dot{W}_c\sqrt{T}}{C_d C P_c f_1\left(\frac{P_s}{P_c}\right)} \quad \text{where } f_1\left(\frac{P_s}{P_c}\right) = f_1\left(\frac{1730}{2215}\right) = 0.860$$

$$A_c = \frac{0.176\sqrt{2460}}{0.87 \times 0.412 \times 2215 \times 0.86} = 0.0128 \text{ in.}^2$$

Vortex Regulator Design

To determine the regulator valve chamber orifice area (A_{sr}), the supply pressure must be known. However, the orifice area A_{br} can be determined since the minimum value of P_s is known:

$$A_{br} = \frac{0.16\sqrt{2460}}{0.87 \times 0.412 \times 1865\, f_1\left(\frac{1730}{1865}\right)} \quad \text{where } f_1\left(\frac{1730}{1865}\right) = 0.545$$

$$A_{br} = 0.0218 \text{ in.}^2$$

and the A_{br}' orifice is calculated:

$$A_{br}' = \frac{0.16\sqrt{2460}}{0.87 \times 0.412 \times 2265\, f_1\left(\frac{1865}{2265}\right)} \quad \text{where } f_1\left(\frac{1865}{2265}\right) = 0.795$$

$$A_{br}' = 0.0123 \text{ in.}^2$$

For P_s' to remain constant, P_s must change to offset the change in $\dot{W}_c$. Substituting the minimum and maximum values for $\dot{W}_{or}$, $\dot{W}_{br}$, $\dot{W}_{op}$ and $\dot{W}_c$ in equation (2) gives:

$$\dot{W}_s \text{ (max.)} = 0.88 \text{ lb/sec}$$

$$\dot{W}_s \text{ (min.)} = 0.792 \text{ lb/sec}$$

$$A_s' = \frac{0.88 \sqrt{2460}}{0.87 \times 0.412 \times 2265 \; f_1\left(\frac{1730}{2265}\right)} \quad \text{where } f_1\left(\frac{1730}{2265}\right) = 0.879$$

$$A_s' = 0.0613 \text{ in.}^2$$

When the flow decreases to 0.792 lb/sec through A_s', P comes:

$$f_1\left(\frac{P_s}{P_s'}\right) = \frac{W_s \text{ (min.)} \sqrt{T_u}}{C_d C A_s' P_s'} = \frac{0.792 \sqrt{2460}}{0.87 \times 0.412 \times 0.0613 \times 2265} = 0.793$$

$$\frac{P_s}{P_s'} = 0.825$$

$$P_s = 0.825 \; (2265) = 1865 \text{ psia}$$

and

$$A_{sr} = \frac{0.792 \sqrt{2460}}{0.87 \times 0.412 \times 1865} = 0.0590 \text{ in.}^2$$

Table A-1 summarizes the system design parameters. Equivalent flow and pressure is determined using equation (5). Table A-2 summarizes the vortex valve configuration and the system orifice sizes.

Table A-2 - Tabulation of Orifice Areas

Regulator	Power Valve	System
$A_{br} = 0.0218 \text{ in.}^2$	$A_c = 0.0128 \text{ in.}^2$	$A_{br}' = 0.0123 \text{ in.}^2$
$A_{sr} = 0.059 \text{ in.}^2$	$A_{sp} = 0.0707 \text{ in.}^2$	$A_s' = 0.0613 \text{ in.}^2$
A_{op} = as required	$A_{op} = 0.136 \text{ in.}^2$	

APPENDIX B

HOT-GAS SECONDARY INJECTION SYSTEM DYNAMIC RESPONSE BY LINEAR ANALYSIS

Summary

The transfer function relating a change in pilot valve area to a change in power valve plenum pressure evaluated at a mid-range operating point is:

$$\frac{P_{op}(s)}{A_9(s)} = -\left\{ \frac{K_1 K_4 (1+\tau_7 s)(K_4 - K_3 K_5 + K_4 \tau_2 s)}{K_1 K_3 K_4 (1+\tau_3 s)(1+\tau_7 s) + K_4 (1+\tau_2 s)(1+\tau_3 s)\left[-K_6 K_7 + (1+\tau_1 s)(1+\tau_7 s)\right]} - \frac{K_5}{1+\tau_3 s} \right\} \frac{K_2}{(1+\tau_2 s)}$$

Table B-1 defines the symbols used in the derivation of the various equations leading to the final transfer function.

Table B-1 - Linear Coefficients

Linear Coefficients	Value
K_1	5.7×10^{-2}
K_2	8.14×10^{4}
K_3	2.72×10^{-2}
K_4	2.72×10^{-2}
K_5	2.52
K_6	5.75×10^{-2}
K_7	9.82×10^{-1}
τ_1	1.575×10^{-4} sec
τ_2	2.04×10^{-4} sec
τ_3	1.05×10^{-3} sec
τ_4	1.02×10^{-3} sec

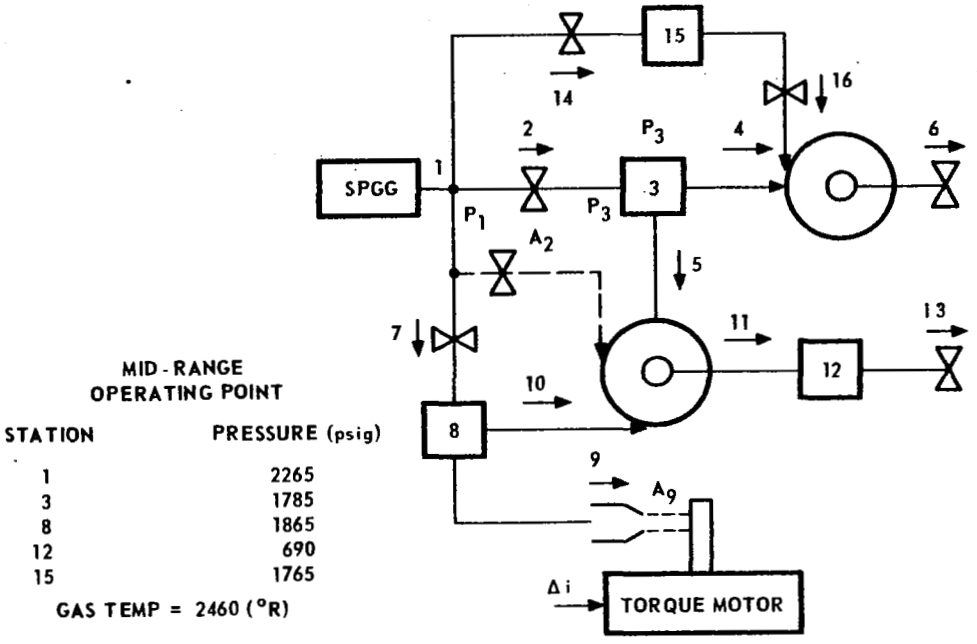

Figure B-1 - System Schematic

System Model

Perturbation equations for the system model shown in Figure B-1 are as follows:

$$\dot{W}_2 - \dot{W}_4 - \dot{W}_5 = c_3 \dot{P}_3 \tag{1}$$

$$\dot{W}_7 - \dot{W}_9 - \dot{W}_{10} = c_8 \dot{P}_8 \tag{2}$$

$$\dot{W}_{11} - \dot{W}_{13} = c_{12} \dot{P}_{12} \tag{3}$$

$$\dot{W}_{14} - \dot{W}_{15} = c_{15} \dot{P}_{15} \tag{4}$$

The perturbation flows for the operating point conditions shown in Figure B-1 are determined from the flow equation:

$$\dot{W} = \frac{C A P_u}{\sqrt{T}} f_1\left(\frac{P_d}{P_u}\right) \tag{5}$$

or by graphical evaluation of the partial derivatives of the vortex valve characteristics curves, as follows:

The weight flow through orifice 2 is given by:

$$\dot{W}_2 = \frac{C A_2 P_1}{\sqrt{T}} f_1\left(\frac{P_3}{P_1}\right)$$

This equation is linearized by differentiating:

$$\Delta\dot{W}_2 = \frac{C A_2 P_1}{\sqrt{T}} f_1'\left(\frac{P_3}{P_1}\right)\Delta P_3$$

The pressure P_1 does not vary; therefore it was only necessary to differentiate with respect to P_3. In this linearized equation, P_3 is considered a constant, or quiescent, pressure and ΔP_3 is the variable part of the pressure. Thus:

$$\Delta\dot{W}_2 = K_{2,3}\,\Delta P_3$$

The subscripts of K represent the flow and pressure. Thus $K_{2,3}$ is the gain term for the change in flow $\dot{W}_2$ resulting from a change in pressure P_3.

The vortex valve flow $\dot{W}_4$ is a function of pressure P_3 and P_{15}.

$$\Delta\dot{W}_4 = \Delta P_3 \left|\frac{\partial\dot{W}_4}{\partial P_3}\right|_{P_{15}=\text{Constant}} + \Delta P_{15}\left|\frac{\partial\dot{W}_4}{\partial P_{15}}\right|_{P_3=\text{Constant}}$$

$$\Delta\dot{W}_4 = K_{4,3}\,\Delta P_3 + K_{4,15}\,\Delta P_{15}$$

These two examples illustrate the method for forming the perturbation flow equations. By definition, perturbation equation implies that the equation represents a change in the dependent variable for a small change, or perturbation, of the independent variable about the quiescent operating point. The following set of perturbation flow equations was derived in the same manner as the two examples shown. (The Δ notation will be dropped for convenience.)

$$\dot{W}_2 = -K_{2,3}\,P_3 \tag{6}$$

$$\dot{W}_4 = K_{4,3}\,P_3 - K_{4,15}\,P_{15} \tag{7}$$

$$\dot{W}_5 = K_{5,3}\,P_3 - K_{5,8}\,P_8 \tag{8}$$

$$\dot{W}_7 = -K_{7,8}\,P_8 \tag{9}$$

$$\dot{W}_9 = K_9 A_9 + K_{9,8} P_8 \tag{10}$$

$$\dot{W}_{10} = K_{10,8} P_8 - K_{10,3} P_3 \tag{11}$$

$$\dot{W}_{11} = K_{11,3} P_3 - K_{11,8} P_8 \tag{12}$$

$$\dot{W}_{13} = K_{13,12} P_{12} \tag{13}$$

$$\dot{W}_{14} = -K_{14,15} P_{15} \tag{14}$$

$$\dot{W}_{16} = K_{16,15} P_{15} - K_{16,3} P_3 \tag{15}$$

The gain terms in the perturbation equations are evaluated as follows:

$$K_{2,3} = -\frac{C A_2}{\sqrt{T}} f_1' \left(\frac{P_3}{P_1}\right) \text{ (All K are positive)} \tag{16}$$

$$K_{4,3} = \left| \frac{\partial \dot{W}_4}{\partial P_3} \right| \tag{17}$$

$$K_{4,15} = \left| \frac{\partial \dot{W}_4}{\partial P_{15}} \right| \tag{18}$$

$$K_{5,3} = \left| \frac{\partial \dot{W}_5}{\partial P_3} \right| \tag{19}$$

$$K_{5,8} = \left| \frac{\partial \dot{W}_5}{\partial P_8} \right| \tag{20}$$

$$K_{7,8} = -\frac{C A_7}{\sqrt{T}} f_1 \left(\frac{P_8}{P_1}\right) \tag{21}$$

$$K_9 = \frac{C P_8}{\sqrt{T}} \tag{22}$$

$$K_{9,8} = \frac{C A_9}{\sqrt{T}} \tag{23}$$

$$K_{10,8} = \frac{C A_{10}}{\sqrt{T}} \left[f_1\left(\frac{P_3}{P_8}\right) - \left(\frac{P_3}{P_8}\right) f_1'\left(\frac{P_3}{P_8}\right) \right] \tag{24}$$

$$K_{10,3} = \frac{C A_{10}}{\sqrt{T}} f_1'\left(\frac{P_3}{P_8}\right) \tag{25}$$

$$K_{11,3} = K_{5,3} \tag{26}$$

$$K_{11,8} = K_{5,8} \tag{27}$$

$$K_{13,12} = \frac{C A_{13}}{\sqrt{T}} \tag{28}$$

$$K_{14,15} = -\frac{C A_{14}}{\sqrt{T}} f_1'\left(\frac{P_{15}}{P_1}\right) \tag{29}$$

$$K_{16,15} = \frac{C A_{16}}{\sqrt{T}} \left[f_1\left(\frac{P_{15}}{P_3}\right) - \frac{P_{15}}{P_3} f_1'\left(\frac{P_{15}}{P_3}\right) \right] \tag{30}$$

$$K_{16,3} = \frac{C A_{16}}{\sqrt{T}} f_1'\left(\frac{P_{15}}{P_3}\right) \tag{31}$$

The pneumatic capacitances are:

$$c_3 = \frac{V_3}{kRT_3} = 3.64 \times 10^{-6} \text{ in.}^2 \tag{32}$$

$$c_8 = \frac{V_8}{kRT_8} = 3.14 \times 10^{-8} \text{ in.}^2 \tag{33}$$

$$c_{12} = \frac{V_{12}}{RT_{12}} = 8.65 \times 10^{-7} \text{ in.}^2 \tag{34}$$

$$c_{15} = \frac{V_{15}}{kRT_{15}} = \frac{4.62}{3.18 \times 10^{6}} = 1.45 \times 10^{-6} \text{ in.}^2 \tag{35}$$

Substituting for the flow terms in equations (1) through (4) gives:

$$-K_{2,3} P_3 - K_{4,3} P_3 + K_{4,15} P_{15} - K_{5,3} P_3 + K_{5,8} P_8 = c_3 \dot{P}_3 \tag{36}$$

$$-K_{7,8} P_8 - K_9 A_9 - K_{9,8} P_8 - K_{10,8} P_8 + K_{10,3} P_3 = c_8 \dot{P}_8 \tag{37}$$

$$K_{11,3} P_3 - K_{11,8} P_8 - K_{13,12} P_{12} = c_{12} \dot{P}_{12} \tag{38}$$

$$-K_{14,15} P_{15} - K_{16,15} P_{15} + K_{16,3} P_3 = c_{15} \dot{P}_{15} \tag{39}$$

Solving equations (36) through (39) for P_3 and P_8 gives:

$$P_3 \left(K_{2,3} + K_{4,3} + K_{5,3} + c_3 s \right) = K_{5,8} P_8 + K_{4,15} P_{15} \tag{40}$$

$$P_3 = \frac{K_1}{1 + \tau_1 s} P_8 + \frac{K_6}{1 + \tau_1 s} P_{15} \tag{41}$$

where:

$$K_1 = \frac{K_{5,8}}{K_{2,3} + K_{4,3} + K_{5,3}} \tag{42}$$

$$\tau_1 = \frac{c_3}{K_{2,3} + K_{4,3} + K_{5,3}} \tag{43}$$

$$K_6 = \frac{K_{4,15}}{K_{2,3} + K_{4,3} + K_{5,3}} \tag{44}$$

$$P_8 = \frac{K_3}{1 + \tau_2 s} P_3 - \frac{K_2}{1 + \tau_2 s} A_9 \tag{45}$$

where:

$$K_2 = \frac{K_9}{K_{7,8} + K_{9,8} + K_{10,8}} \tag{46}$$

$$\tau_2 = \frac{c_8}{K_{7,8} + K_{9,8} + K_{10,8}} \tag{47}$$

$$K_3 = \frac{K_{10,3}}{K_{7,8} + K_{9,8} + K_{10,8}} \tag{48}$$

$$P_{12} = \frac{K_4}{1 + \tau_3 s} P_3 - \frac{K_5}{1 + \tau_3 s} P_8 \tag{49}$$

$$K_4 = \frac{K_{11,3}}{K_{13,12}} \tag{50}$$

$$\tau_3 = \frac{c_{12}}{K_{13,12}} \tag{51}$$

$$K_5 = \frac{K_{11,8}}{K_{13,12}} \tag{52}$$

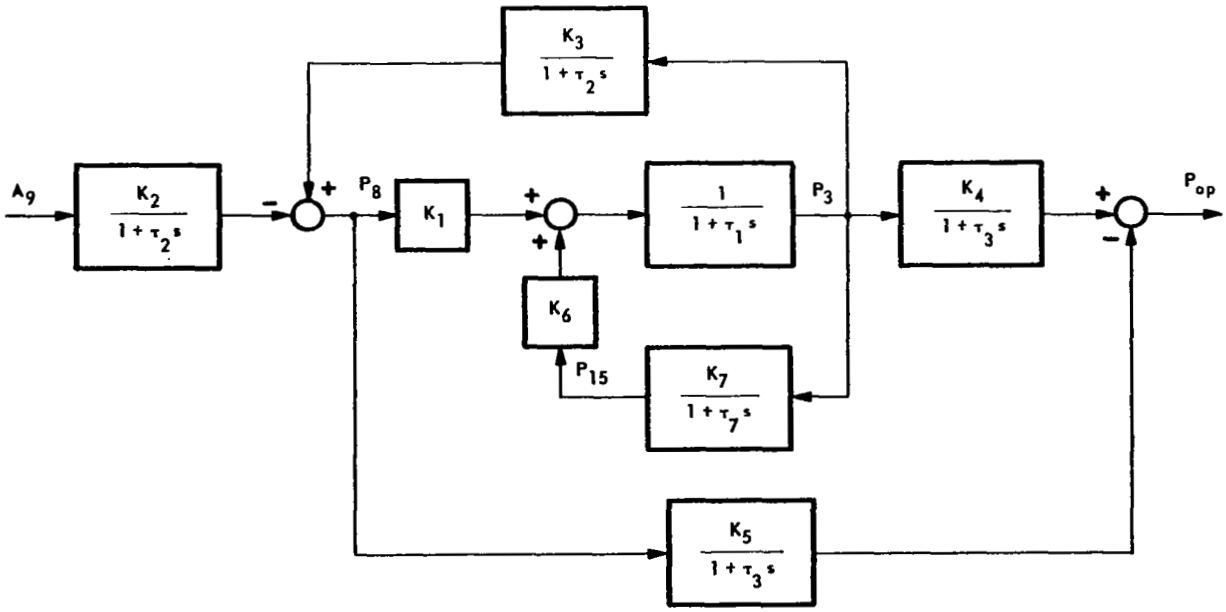

Figure B-2 - System Block Diagram

$$P_{15} = \frac{K_7}{1 + \tau_7 s} P_3 \tag{53}$$

$$K_7 = \frac{K_{16,3}}{K_{14,15} - K_{16,15}} \tag{54}$$

$$\tau_7 = \frac{c_{15}}{K_{14,15} - K_{16,15}} \tag{55}$$

These equations define the dynamic response of the four pressure variables P_3, P_8, P_{12} and P_{15} (Figure B-2).

Reduction of the block diagram in Figure B-2 provides the linear coefficients for the mid-range operating point from which the transfer function is plotted. The frequency response is approximately the same as for a single order system with a break frequency of 311 radians per second for cold gas and 732 radians per second for hot gas.

BIBLIOGRAPHY

Emswiler, J. E., Schwartz, F. L., "Thermodynamics," Mc-Graw-Hill Book Company, Inc., New York and London, 1943.

Mayer, E. A., and Maker, P., "Control Characteristics of Vortex Valves," Bendix Corporation, Research Laboratories Division, Proceedings of the Second Fluid Amplification Symposium, Harry Diamond Laboratories, Washington, D. C., May 1965.

Sutton, G. P., Rocket Propulsion Elements, John Wiley and Sons, Inc., 1965.

REFERENCES

(1) Taplin, L. B., "Phenomenology of Vortex Flow and its Application to Signal Amplification," Bendix Corporation, Research Laboratories Division; Presented at Pennsylvania State University, Summer Engineering Seminars, Fluid Control Systems; July 6-16, 1965.

(2) Blackburn, Reethof and Shearer; Fluid Power Control, John Wiley and Sons, Inc., 1960.

ABSTRACT

A feasibility demonstration of the vortex valve principle and its application to the modulation of the flow of a 2000°F solid propellant gas was investigated. In particular, its application to a hot-gas secondary injection thrust vector control system was considered. Cold-gas scale model vortex valves were tested to derive parametric relationships for final hardware design. Prototype models were then designed and tested with both cold gas and 2000°F hot gas from a solid propellant gas generator. The investigation included five 30-second hot-gas system tests which demonstrated total flow modulation, dynamic response, and hardware design.

NASA-Langley, 1966 CR-424